



## Application of a Markov Chain Monte Carlo algorithm for snow water equivalent retrieval from passive microwave measurements



Jinmei Pan <sup>a,\*</sup>, Michael T. Durand <sup>a</sup>, Benjamin J. Vander Jagt <sup>a</sup>, Desheng Liu <sup>b</sup>

<sup>a</sup> School of Earth Science and Byrd Polar and Climate Research Center, Ohio State University, OH 43210, USA

<sup>b</sup> Department of Geography, The Ohio State University, OH 43210, USA

### ARTICLE INFO

#### Article history:

Received 11 May 2016

Received in revised form 27 January 2017

Accepted 11 February 2017

Available online xxxx

#### Keywords:

Passive microwave remote sensing

Snow water equivalent

Retrieval algorithm

### ABSTRACT

Recent applications of passive microwave remote sensing techniques to estimate snow water equivalent (SWE) increasingly rely on the comprehension of microwave emission theories, instead of traditional empirical fitting approaches. In this study, an advanced SWE retrieval algorithm based on the Markov Chain Monte Carlo method was developed. This method samples the posterior multiple-layer snow properties according to the likelihood of the brightness temperature ( $T_B$ ) simulation with the actual  $T_B$  observations. The Microwave Emission Model of Layered Snowpacks with improved Born approximation (MEMLS-IBA) was used as the observation model. Using a globally applicable method to produce prior estimates of snow properties, the retrieval approach is called the Bayesian Algorithm for SWE Estimation with Passive Microwave measurements (BASE-PM), and was applied on 48 snowpits at Sodankylä, Finland; Churchill, Canada and Colorado, US. The result shows that the root mean squared (RMS) error of the retrieved SWE is 42.7 mm excluding two outliers, and is 30.8 mm if the outliers as well as six deep snowpits from Colorado are excluded. This accuracy approximately meets the 30-mm requirement of Integrated Global Observing Strategy for shallow snow. The poor performance for the outlier and deep snowpits is explained. Additional experiments using more accurate priors show that SWE retrieval accuracy can be improved with local snowcover knowledge, e.g. if historical snowpit measurements or snow process model simulations are available.

© 2017 Elsevier Inc. All rights reserved.

### 1. Introduction

Estimation of the water resources stored inside snow cover is important for water resource management, as well as meteorological and climatological applications (Pulliajainen and Hallikainen, 2001; Tedesco et al., 2004). Passive microwave brightness temperature ( $T_B$ ) has a long history of use for snow water equivalent (SWE) retrieval, due to its short revisit time, global coverage, and its ability to penetrate clouds (Grody and Basist, 1996; Foster et al., 2009). The theory of SWE retrieval from  $T_B$  measurements relies on volume scattering produced by the highly-irregular porous snow medium at high frequencies (Ulaby and Long, 2014). However, SWE retrieval is a very difficult task, not least because the size of the scattering particles has a strong influence on the magnitude of volume scattering (Armstrong et al., 1993; Kelly et al., 2003). Indeed, according to snow emission models (Wiesmann and Matzler, 1999; Liang et al., 2008; Lemmetyinen et al., 2010; Picard et al., 2013),  $T_B$  observed at the snow surface is a function of a large number of snow parameters, including snow depth, snow grain size, snow density, snow temperature, snow liquid water content, and the background emission beneath the snow. Snow stratigraphy also has non-

negligible effects on the observed  $T_B$  (Durand et al., 2011; Pan et al., 2012). Different layer combinations of the unknown snow properties can also produce similar  $T_B$  responses, which further complicate the inversion problem.

Traditional inversion algorithms are based on empirical relationships between  $T_B$  (typically at multiple frequencies) and SWE. It was first assumed that at high frequencies, the increased amount of scattering would result in a lower  $T_B$ ; thus, the  $T_B$  difference between low and high frequencies can be related to snow depth or SWE (Chang et al., 1987). The empirical relationship between  $T_B$  and SWE can be adjusted according to different snow grain size or land surface cover types. The differences in band choice and coefficient determination result in a series of static and dynamic algorithms, as summarized in Clifford (2010), Frei et al. (2012) and Jiang et al. (2014). More sophisticated SWE estimation algorithms have since been developed, which rely on snow emission models to find the snow properties that match the observed  $T_B$ . Data assimilation methods couple the snow emission model with the snow process model into a probabilistic-based dynamic model; these methods are not reviewed here; see Andreadis and Lettenmaier (2012) for more details.

Of all the previous SWE estimation algorithms, the physically based retrieval algorithms using only microwave measurements can be classified into search-based methods and signal-decomposition methods. In

\* Corresponding author.

E-mail address: [jinmei.pan@gmail.com](mailto:jinmei.pan@gmail.com) (J. Pan).

search-based methods,  $T_B$  signals are simulated using random combinations of snow parameters, and the best combination which gives a simulated  $T_B$  signal closest to the observations is chosen as the retrieval result. The accuracy and the efficiency of this procedure are determined by the algorithm utilized. Some examples are the simple searching methods (Pulliainen et al., 1999; Roy et al., 2004; Butt and Kelly, 2008; Butt, 2009), simple searching methods with prior information (Pulliainen, 2006; Takala et al., 2011), Artificial Neural Network (ANN) methods (Davis et al., 1993; Tedesco et al., 2004; Gan et al., 2009), and Genetic Algorithm (GA) (Tedesco and Kim, 2006). In these methods, one-layer Helsinki University of Technology (HUT) model (Pulliainen et al., 1999) and one-layer Dense Media Radiative Transfer (DMRT) model under quasi-crystalline approximation with coherent potential (QCA-CP) (Tsang and Kong, 2001) were used as the observation model. Prior information has been used in SWE retrieval. For example, Takala et al. (2011) estimates an effective snow grain size at station locations where SWE is known and interpolates it to nearby pixels as the grain size prior. The signal-decomposition methods utilize the empirical relationships found in physically-based snow emission model simulation datasets. Jiang et al. (2007) used two-frequency, dual-polarization  $T_B$  to separate the emission from snow volume scattering and the emission from the underlying soil, and fit the SWE as a function of the snow emission. Examples using multi-angle radar measurements can be found in Du et al. (2010).

In this paper, our goal is to build a physically-based SWE retrieval algorithm allowing for multi-layer snowpack and prior information on the snow properties. In general, it can be classified as a search-based method with priors. In our algorithm, the Markov Chain Monte Carlo (MCMC) method (Gelman et al., 1995) was applied to choose snow parameters that give the same simulated  $T_B$  as the observed values, while taking the prior information into account in a Bayesian sense. We call it the Bayesian Algorithm for SWE Estimation with Passive Microwave measurements (BASE-PM). BASE-PM applies the same SWE retrieval method introduced in Durand and Liu (2012), but we used actual  $T_B$  observations from ground-based radiometers, rather than synthetically generated  $T_B$  estimates. As mentioned in Durand and Liu (2012), prior information is required in MCMC to prevent snow variables going beyond their reasonable range in natural snowcover. Therefore, we introduce a method to determine prior snowpack properties from globally available datasets; we refer to these as “generic priors”, as they represent estimates of snow parameters and their uncertainty that are available globally. BASE-PM is also able to utilize locally-derived prior information, such as historical snowpit measurements in the area; we refer to these as “local priors” hereafter, and compare algorithm accuracy using the generic and local priors. Additional features of the BASE-PM algorithm are layered estimates of all snowpack variables (i.e., density, layer thickness, grain size, and soil properties), and an estimate of SWE uncertainty. In this paper, we evaluate BASE-PM; our specific research questions are:

- (1) Can BASE-PM using the generic prior provide SWE estimates that meet the Integrated Global Observing Strategy (IGOS, 2007) requirement for shallow snow, which is 30 mm root mean squared (RMS) error?
- (2) How does the SWE prior influence SWE estimate accuracy?
- (3) How does the prior for the stratigraphy information (layered density, temperature and grain size) influence the accuracy of the estimated SWE?

In this paper, Section 2 introduces observation models and the microwave theory that supports the SWE retrieval; Section 3 introduces the theory and the implementation of the BASE-PM algorithm; Section 4 describes data utilized in this paper; Section 5 explains the detailed methodologies to calculate the priors and to set up the retrieval algorithm. Sections 6, 7 and 8 are Results, Discussions and Conclusions, respectively.

## 2. Microwave emission theory and emission models

Absorption and volume scattering in snowpacks and surface scattering at the snow-soil boundary and snow-layer interfaces determine snowpack brightness temperature ( $T_B$ ) (Wiesmann and Matzler, 1999; Liang et al., 2008; Lemmetyinen et al., 2010; Picard et al., 2013).

Based on the ratio of the wavelength relative to the geometry of the snow micro-structure, scattering tends to dominate at microwave frequencies. Microwave radiation emitted by the soil is scattered to other directions, decreasing  $T_B$  in the observation direction. Based on the assumptions of discrete snow particles (Tsang et al., 2007; Hallikainen et al., 1987) or bi-continuous snow medium (Wiesmann et al., 1998; Matzler and Wiesmann, 1999; Ding et al., 2010; Xu et al., 2012), volume scattering at different frequencies has been measured and modeled via microwave multiple-scattering physics. A critical input is the snow micro-structure parameters (e.g. Matzler, 2002), such as geometric grain size and snow auto-correlation functions. Soil properties provide the background radiation prior to snow attenuation. Vertically-polarized  $T_B$  decreases with the increased soil surface roughness and soil moisture content.

Typically, for homogenous snow,  $T_B$  at the snow surface decreases with increasing SWE and gradually becomes saturated for thick snow (Pan et al., 2016). However, Matzler et al. (1982) and Derksen et al. (2010) observed an increasing  $T_B$  trend after the saturation point for natural snowpacks.

Snow properties are not vertically homogenous within natural snowpacks. Commonly, old snow with depth hoar and refrozen crusts is located beneath new snow with smaller grain size (Lemmetyinen et al., 2016). Snow stratigraphy needs to be considered due to different penetration depths of microwave at different frequencies (Liang et al., 2008). Therefore, we hypothesize that, for SWE retrieval, we also need to consider multi-layer snow properties. We note that, this concern of snow stratigraphy in microwave simulations can be different with the requirements of snow process models, which are not directly used in BASE-PM.

In the algorithm we present in this paper, we take microwave emission theory into account by using physically-based radiative transfer models in the iterative estimation framework. We utilized the Microwave Emission Model of Layered Snowpacks (MEMLS) based on the improved Born approximation (Matzler and Wiesmann, 1999) for snow emission calculation, the rough bare soil reflectivity model (Wegmüller and Matzler, 1999) for soil emission calculation, and the semi-empirical soil dielectric constant model (Dobson et al., 1985) for soil permittivity calculation.

MEMLS is a 6-flux snow radiative transfer emission model. It calculates  $T_B$  of multiple-layer snowpacks with layered information of snow thickness, density, temperature, and exponential correlation length ( $p_{ec}$ ).  $p_{ec}$  is the parameter used to describe snow micro-structure in MEMLS, based on the assumption of a continuous snow medium irregularly occupied by air and ice components. Although there are other physically-based snow emission models, like the Dense Media Radiative Transfer (DMRT) models (Tsang et al., 2007; Ding et al., 2010; Picard et al., 2012), we will start with MEMLS-IBA that has been proven to predict the  $T_B$  observations well at the same sites (Pan et al., 2016).

The rough bare soil reflectivity model calculates the soil emission as a function of soil temperature, roughness (root-mean-squared height) and soil permittivity. The Dobson semi-empirical model requires soil moisture (volumetric water content), soil temperature, soil bulk density, and soil texture to calculate snow permittivity. Here, a simplification is made to estimate only soil roughness, soil temperature and soil moisture in BASE-PM. The soil bulk density is fixed as 1.5 g/cm<sup>3</sup>; soil texture is fixed as 30.63% sand, 55.89% silt and 13.48% clay, which is a medium texture for experiments in Hallikainen et al. (1985). The original Dobson model does not treat frozen soil. Thus, the estimated soil moisture must be considered to be an effective value if soil temperature is below the

freezing point, since freeze-thaw state changes soil permittivity (Mironov et al., 2010).

### 3. BASE-PM SWE retrieval algorithm

#### 3.1. The MCMC theory

When the number of  $T_B$  measurements is significantly smaller than the number of estimated snow and soil variables, some prior information of these variables is required to reduce the uncertainty in the SWE retrieval.

The Markov Chain Monte Carlo (MCMC) method is based on Bayesian statistical theory, and is a numerical realization of Bayes' law. In our application, we use MCMC to find a combination of estimated snowpack variables that gives the highest possible posterior probability. The latter is based both on the difference between the observed and the simulated  $T_B$ , and the difference between estimated snowpack variables and their prior estimates. We define a vector containing all the estimated variables mentioned in Section 2  $\theta$ , and a vector containing the multi-frequency  $T_B$  measurements  $y$ , where  $y = [T_{B,f1}, T_{B,f2}, \dots]$ . The posterior probability of  $\theta$  conditioned on the  $T_B$  measurements is therefore described as  $p(\theta|y)$ . When  $p(\theta|y)$  is maximized, then it is most likely that this  $\theta$  is close to true snowpack conditions. According to Bayes' law,  $p(\theta|y)$  can be calculated as (Gelman et al., 1995):

$$p(\theta|y) = \frac{p(\theta)p(y|\theta)}{p(y)} \quad (1)$$

In this equation,  $p(y) = \sum_\theta p(\theta)p(y|\theta)$ , which is the sum of  $T_B$  over all possible values of  $\theta$ .  $p(y)$  is invariant for a particular snowpit, and thus its calculation can be avoided, as described below.  $p(\theta)$  is the prior probability of the snow and soil parameters for a particular snowpit.  $p(y|\theta)$  is the probability of the observed  $T_B$  given  $\theta$ : it is essentially just a statistical model of the observation error. Assumed the  $T_B$  observation error follows a multi-variate normal distribution,  $p(y|\theta)$  can be calculated as (Durand and Liu, 2012):

$$p(y|\theta) = (2\pi)^{-\frac{N_y}{2}} |\Sigma_y|^{-\frac{1}{2}} \exp \left[ -\frac{1}{2} (y - M(\theta))^T \Sigma_y^{-1} (y - M(\theta)) \right] \quad (2)$$

where  $N_y$  is the number of frequencies in  $T_B$  measurements,  $\Sigma_y$  is the  $T_B$  error covariance matrix, and  $M(\theta)$  is the observation model mentioned in Section 2.  $M(\theta)$  calculates the simulated  $T_B$  based on  $\theta$ . Thus, the snow microwave emission physics is involved in retrieval via the comparison of  $y$  and  $M(\theta)$ .

The MCMC algorithm computes  $p(\theta|y)$  by starting from an initial combination of snowpack variables, and using a "likelihood ratio" to guide the estimate into the region of the parameters space where the snowpack variables best represent the observed  $T_B$ . The algorithm uses a "random walk" approach. At each iteration of the Markov Chain,  $\theta_{i-1}$  represents snowpack variables before the random walk, and  $\theta_{i,\text{candidate}}$  is produced using a so-called "jump distribution". Then,  $p(\theta_{i-1}|y)$  and  $p(\theta_{i,\text{candidate}}|y)$  can be compared using:

$$r = \frac{p(\theta_{i,\text{candidate}}|y)}{p(\theta_{i-1}|y)} = \frac{p(\theta_{i,\text{candidate}})p(y|\theta_{i,\text{candidate}})}{p(\theta_{i-1})p(y|\theta_{i-1})} \quad (3)$$

$r$  is the likelihood ratio (Gelman et al., 1995); note that  $p(y)$  has been eliminated. If  $r$  is larger than 1, then  $\theta_{i,\text{candidate}}$  is more likely to have produced the observed  $T_B$ , and thus we will accept it as the chosen  $\theta_i$  at the current  $i$ -th iteration, and use it as the starting point for the next iteration. If  $r$  is smaller than 1, then we will probabilistically determine whether to accept or reject the current candidate, with an  $r$  percent chance that the candidate  $\theta$  will be accepted. If the candidate is rejected, we will set  $\theta_i$  as the same as  $\theta_{i-1}$ , and wait for the next iteration to test another jumping direction.

Fig. 1 shows a schematic view of the flow chart at iteration  $i$ . At the  $i$ th iteration, to update  $\theta_i$ , we use a symmetric jump function,  $J(\theta_i) = \theta_{i-1} + d\theta_i$ , where,  $d\theta_i$  is a normally-distributed random number centered at zero and a standard deviation referred to as the jump size. The jump size is adaptively tuned to provide the optimal acceptance rate. For the multi-layer snow case, the snow thickness, temperature, density and micro-structure parameter are updated in blocks (i.e., for example, thicknesses for all layers are updated at one time) to avoid joint jump functions.

After a large number of iterations, a Markov chain will be built, which numerically sampled the snow properties that can reproduce the  $T_B$  measurements, except the first several iterations that are still influenced by the initial values. These iterations are called the burn-in period. SWE and the estimated snow variables can be summarized from the Markov chain after the burn-in period.

#### 3.2. The BASE-PM implementation

In Durand and Liu (2012), the MCMC algorithm used 10,000 iterations; the first 2000 iterations were considered the burn-in period, and the remainder of the chain was used to compute the posterior  $\theta$ . We will revisit chain length in the present study, and will check chains for convergence (Gelman et al., 1995).

The inputs to the MCMC algorithm for a given snowpit are the  $T_B$  observations and the priors of the estimated variables; the output is the posterior Markov chain of the estimated variables. Here, we assume that the error of the measured  $T_B$  is 2 K; see Section 3 for details. The estimated variables are layered snow thickness, density, temperature, micro-structure parameter, as well as soil roughness, temperature and moisture. In a multi-layer snowpack,  $p(\theta|y)$  is calculated including a probability of the number of layers,  $n_{lyr}$ ; see Eq. (4) in Durand and Liu (2012). It assumed the prior distribution of  $n_{lyr}$  follows a Poisson distribution.

According to Durand and Liu (2012) and the analysis of the in-situ measurements, it is reasonable to assume the priors of snow and soil parameters follow log-normal distributions. A log-normal distribution is useful when valid values of a parameter are all positive (e.g. snow depth, density,  $p_{ec}$ ) or negative (e.g. snow temperature). If a variable  $x$  follows a log-normal distribution with a mean of  $\mu_x$  and a standard deviation of  $\sigma_x$ ,  $\log(x)$  will follow a normal distribution with its mean ( $\mu_{\log x}$ ) and standard deviation ( $\sigma_{\log x}$ ) given by:

$$\mu_{\log x} = \log \left[ \frac{\mu_x^2}{\sqrt{\mu_x^2 + \sigma_x^2}} \right] \quad (4)$$

$$\sigma_{\log x} = \sqrt{\log \left( \frac{\sigma_x^2}{\mu_x^2} + 1 \right)} \quad (5)$$

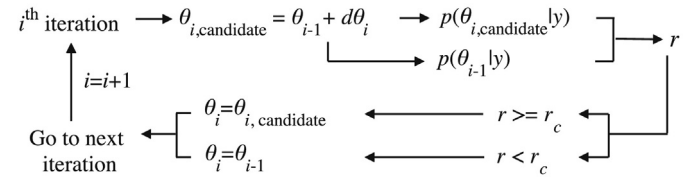


Fig. 1. A schematic view of the flow chart of the MCMC algorithm at the  $i$ th iteration. It starts from a random walk to produce a candidate combination of snow/soil estimates ( $\theta_{i,\text{candidate}}$ ) using  $\theta_{i-1}$  from the last iteration.  $\theta$  includes multi-layer snow thickness, temperature, density, exponential correlation length, and soil temperature, soil volumetric moisture and soil surface roughness. Then, we calculate the posterior probability ( $p(\theta|y)$ ) of  $\theta_{i,\text{candidate}}$  and  $\theta_{i-1}$  conditioned on the multi-frequency  $T_B$  measurements ( $y$ ).  $r$  is the likelihood ratio of  $p(\theta_{i,\text{candidate}}|y)$  to  $p(\theta_{i-1}|y)$  defined in Eq. (3). The algorithm will determine the final estimates at  $i$ -th iteration ( $\theta_i$ ) according to  $r$  with relevant to a probabilistic value,  $r_c$ .

Note that snow and soil temperatures ( $T$  in K) are converted to 274 K –  $T$  to be used in Eqs. (4) and (5).

The local priors are computed from statistics of snowpit measurements. For SWE, the local prior was computed from the monthly-average SWE of all snowpits at each site. The local priors for density, temperature and grain size metrics were computed from layered snow property measurements. The Markov chain was first built for each  $n_{lyr}$  independently. Then, the estimates of 1-, 2- and more layers were compared using Eq. (5) in Durand and Liu (2012). To compute priors for a certain  $n_{lyr}$ , snowpit measurements were relayed to  $n_{lyr}$  following the method in Jordan (1991).

The generic priors are computed from globally available datasets. We used the monthly average SWE from historical land surface model predictions, and we set the generic priors of density, temperature and grain size metrics according to snow types (Sturm et al., 1995). The details of the datasets used to calculate the priors will be later shown in Section 4. Because RT model usually uses layer thickness instead of SWE, the SWE and density priors are used to compute a prior on snow depth (SD), and layer thickness (dz) using the following equations (Van Kempen and Van Vliet, 2000):

$$\mu_{SD} = \frac{\mu_{SWE}}{\mu_{\rho_b}} \quad (6)$$

$$\sigma_{SD}^2 = \frac{\mu_{SWE}^2}{\mu_{\rho_b}^2} \left[ \frac{\sigma_{SWE}^2}{\mu_{SWE}^2} - 2 \frac{r_{SWE,\rho_b} \sigma_{SWE} \sigma_{\rho_b}}{\mu_{SWE} \mu_{\rho_b}} + \frac{\sigma_{\rho_b}^2}{\mu_{\rho_b}^2} \right] \quad (7)$$

$$\mu_{dz} = \frac{\mu_{SD}}{n_{lyr}} \quad (8)$$

$$\sigma_{dz}^2 = \frac{\sigma_{SD}^2}{n_{lyr}} \quad (9)$$

where,  $\rho_b$  is the bulk density of the snowpit.  $r_{SWE,\rho_b}$  is the Pearson's correlation coefficient between SWE and  $\rho_b$ . In this paper, the covariance of SWE and bulk density can be different according to the generic or local prior options; however, the correlation between them was fixed as 0.3, which was calculated from all snowpits at three sites.

On the first iteration, we set the initial  $\theta_0$  as  $\exp(\mu_{logx} + 0.5\sigma_{logx}^2)$  for all variables. Then, the procedures shown in Fig. 1 are performed iteratively. After the MCMC chains of all estimated variables are produced, and the  $n_{lyr}$  with highest posterior probability is chosen compared to other number of layers, a chain of SWE is calculated using the chains of layered density and thickness estimates. The MCMC-estimated SWE is calculated across the chain via:

$$SWE_{MCMC} = \exp \left( \frac{1}{i_{total} - i_{burn-in}} \sum_{i=i_{burn-in}+1}^{i_{total}} \log(SWE_i) \right) \quad (10)$$

where,  $SWE_i$  is SWE at the  $i$ -th iteration.  $i_{total}$  is the total length of the MCMC chain.  $i_{burn-in}$  is the length of the burn-in period. This equation is used because the SWE chain follows a log-normal distribution. The use of  $\exp(\mu_{logx})$  reduces the influence of extreme values at the right tail of the distribution.

The uncertainty of MCMC-estimated SWE is calculated as:

$$\sigma_{SWE,MCMC} = \sqrt{\frac{1}{i_{total} - i_{burn-in}} \sum_{i=i_{burn-in}+1}^{i_{total}} (SWE_i - SWE_{MCMC})^2} \quad (11)$$

The MCMC-estimates of other variables can be calculated using similar methods.

## 4. Data

Experiments run in this paper utilize data from three sites, including Sodankylä, Finland; Churchill, Canada; and the Local Scale Observation

Site (LSOS) during the Cold Land Processes Field Experiment (CLPX), located in the central Rocky Mountains in Colorado, USA. There are 48 snowpits in total, each with concurrent  $T_B$  observations: 36 from Sodankylä, 6 from Churchill and 6 from CLPX-LSOS. In this section, we introduce the data utilized for SWE retrieval, including the  $T_B$  measurements (Section 4.1), the snowpit measurements used for local prior calculation (Section 4.2) and the datasets used for generic prior calculation (Section 4.3).

### 4.1. $T_B$ measurements

All  $T_B$  data used for SWE retrieval is from ground-based radiometers. At Sodankylä, the  $T_B$  measurements were observed by Sodankylä Radiometer (SodRad) (Lemmettyinen et al., 2016) at 10.65, 18.7, 36.5 and 90 GHz with an incidence angle of 50° in the first two winters (2009/2010 and 2010/2011) of the Nordic Snow Radar Experiment (NoSREX) campaign. At Churchill, the  $T_B$  measurements were observed by Environment Canada (EC) sledge-based radiometer (Derksen et al., 2012) at 6.9, 19, 37 and 89 GHz with an incidence angle of 53°. At CLPX-LSOS, the  $T_B$  measurements were observed by Ground Based Passive Microwave Radiometer (GBMR-7) (Graf et al., 2003) at 18.7, 36.5 and 89 GHz with an incidence angle of 55°. No satellite or air-borne  $T_B$  was used. Therefore, factors such as forest cover were not considered. Also, only the vertically-polarized  $T_B$  was used, due to the strong influence of ice layers on horizontally-polarized  $T_B$  (Montpetit et al., 2013). The measurement error of the  $T_B$  measurements is about 2 K (Lemmettyinen et al., 2016; Derksen et al., 2012; Graf et al., 2003).

### 4.2. Snowpit measurements

Snowpit measurements are used to validate the SWE estimates, and to calculate the local priors of snow variables. The local prior consists of the mean and the standard deviation of the snowpack variables from historical snowpit measurements.

At Sodankylä, 107 snowpits in forest clearings were observed in four subsequent winters from 2009 to 2013, with a snow type of taiga snow. The 36 snowpits used for retrieval are all dry snowpits with complete  $T_B$  and snow property measurements in the first two winters (2009/2010 and 2010/2011). Note that in the winters of 2011/2012 and 2012/2013, 23-GHz radiometer was operated instead of 90-GHz.

At Churchill, we used 49 measured snowpits (Montpetit et al., 2013; Derksen et al., 2012). They are from the Canadian Cold Regions Hydrology High-Resolution Observatory (CoReH<sub>2</sub>O) Snow and Ice Experiment and the follow-on experiments, but cover all types of snow in the Churchill area, including deep taiga snow, tundra snow, snow over dry/wet fen and snow over lake ice. Only 6 snowpits measured in forest clearings (taiga snow type) were used for SWE retrieval.

At CLPX-LSOS, the 6 snowpits from the week of February 19–26, 2003 during the 3rd Intensive Observation Period (IOP-3) (Cline et al., 2003) are used for retrieval. The snow type there is alpine snow. We compute the prior from 73 ISA snowpits from the Fraser MesoCell Study Area (MSA) measured in February, a 25-km × 25-km region that contains the LSOS, along with a wide range of other snow conditions (Elder et al., 2003).

**Table 1** lists the mean and the standard deviation of SWE and mass-weighted average density, temperature and exponential correlation length ( $p_{ec}$ ) for all snowpits at different months.  $p_{ec}$  was converted from the geometric grain size ( $D_{max}$ ) using the same methods in Pan et al. (2016). It can be seen from **Table 1** that, the standard deviation of SWE varies from 17% to 41% of the mean SWE at different months and sites. However, note that sample sizes are rather small, in some cases. Therefore, for experimental purpose, we set the standard deviation of the local SWE prior as 40% of the measured mean SWE. In other words, we assumed the local SWE prior has a 40% relative accuracy for all cases.

**Table 1**

Statistics of SWE and the mass-weighted average density, temperature and micro-structure parameters of the measured snowpits.

Site, Month	SWE (mm)		Density ( $\text{kg}/\text{m}^3$ )		Temperature ( $^\circ\text{C}$ )		Geometric grain size (mm)		Exponential correlation length (mm)		N	
	Mean	Std	Mean	Std	Mean	Std	Mean	Std	Mean	Std		
CLPX-LSOS Churchill	Feb	185.08	75.67	222.85	35.71	-4.12	1.38	1.33	0.54	0.174	0.041	73
	Jan	112.42	22.64	239.82	29.78	-8.86	2.37	1.61	0.16	0.203	0.015	5
	Feb	137.19	36.96	279.91	57.04	-11.04	4.62	2.80	1.17	0.236	0.041	17
	Mar	179.14	70.93	296.53	31.18	-9.68	5.91	2.04	1.06	0.214	0.053	16
	Apr	149.99	51.90	321.64	50.80	-3.28	2.07	1.94	1.31	0.206	0.052	7
	Nov	54.71	13.27	222.03	29.66	-3.39	3.11	0.80	0.22	0.175	0.049	8
	Dec	75.82	21.99	219.98	31.88	-3.06	3.33	1.05	0.32	0.205	0.042	27
	Jan	110.29	25.31	218.59	30.72	-5.89	2.21	1.40	0.38	0.236	0.041	21
	Feb	150.13	30.91	234.30	36.12	-8.04	4.44	1.35	0.30	0.238	0.032	18
	Mar	173.83	29.12	227.64	18.95	-6.23	3.10	1.38	0.21	0.158	0.044	33

### 4.3. Generic prior datasets

Unlike the local prior, the generic prior is from a set of globally available datasets. The generic prior for SWE is from the global Variable Infiltration Capacity (VIC) Macro-scale Hydrologic Model predictions (Nijssen et al., 2001). VIC uses the time-series meteorological measurements to estimate the evolution of snowpack, including snow accumulation and the increase of SWE from snowfall, and the snow ablation due to snowmelt, driven by surface mass and energy balances. The spatial resolution is 2-degree, and the time range is from 1980 to 1993 (<http://vic.readthedocs.org/en/master/>). Monthly-averaged 2-degree VIC SWE was used for prior estimate at Sodankylä and Churchill. At LSOS, however, we found a 2-degree resolution is too coarse to capture the snow accumulation in mountain. It gives a SWE of  $6.6 \pm 6.2$  mm in February, but the mean SWE from snowpit measurements is 185.08 mm (see Table 1). In this case, we used the 0.125-degree SWE simulated by VIC model driven by the North American Land Data Assimilation System (NLDAS), Phase 2 for the CPLX-LSOS site. The data is downloaded from NLDAS-2 Monthly Climatology datasets (Mocko, 2014).

Table 2 lists the monthly-average SWE for different months. Comparison between Tables 1 and 2 shows that, the SWE predicted by VIC model is underestimated by about 30% to 58% compared to the locally-measured SWE. Therefore, we set the standard deviation of the generic SWE prior as 100% of the VIC SWE. The ratio of standard deviation to the mean is higher for the generic prior, reflecting the lack of precision currently available for global SWE estimates.

The generic priors of snow density and temperature are determined according to typical snow classification system (Sturm et al., 1995). At Sodankylä and Canada, the snowpits we used for retrieval are classified as taiga snow, and the snowpits at CPLX-LSOS are classified as alpine snow. Therefore, the priors are chosen strictly according to the snow

type. Sturm et al. (2010) presents a bulk density of  $217 \pm 56 \text{ kg}/\text{m}^3$  for 1541 taiga snowpits, and a bulk density of  $335 \pm 86 \text{ kg}/\text{m}^3$  for 4623 alpine snowpits. These values were used directly as  $\mu_x$  and  $\sigma_x$  in Eqs. (4) and (5);  $x$  represents density in this case. Sturm et al. (1995) shows the lower bound of the air temperature for taiga snow is  $-21^\circ\text{C}$ , and the upper bound of the soil-snow interface temperature is  $0^\circ\text{C}$ . Therefore, we assumed the prior of snow temperature for taiga snow is  $-10.5 \pm 10.5^\circ\text{C}$ . The prior of snow temperature for alpine snow is  $-6.5 \pm 6.5^\circ\text{C}$ , as determined by the same method.

For the snow micro-structure information not provided by Sturm's classes, the generic prior for  $p_{ec}$  was assumed to be  $0.18 \pm 0.18$  mm. It was determined according to the measurements published in Matzler (2002), where  $p_{ec}$  of fresh snow is about 0.03 mm, and  $p_{ec}$  of depth hoar is about 0.32 mm. As a log-normal distributed variable, a mean and standard deviation of 0.18 mm for  $p_{ec}$  correspond to a range of 0.05–0.29 mm if one standard deviation around the mean of  $\log(p_{ec})$  is considered. According to Durand et al. (2008), a 0.18-mm  $p_{ec}$  is approximately equivalent to a 1-mm geometric grain size ( $D_{max}$ ).

When SWE was estimated using multiple layers, the same generic priors of density, temperature and  $p_{ec}$  were used for different layers. However, we constrained the density of surface layer is no larger than the bottom layer, and the temperature is surface layer is no higher than the bottom layer.

### 5. The experiments

Fig. 2 lists an example of the local and generic priors for a snowpit observed at Sodankylä on March 2<sup>nd</sup>, 2010. Fig. 2(a) shows the in-situ snow measurements. The measured snowpit has 6 layers. The density was  $109.1 \text{ kg}/\text{m}^3$  at the surface layer, and it increased to  $275.75 \text{ kg}/\text{m}^3$  at the bottom layer. The  $p_{ec}$  converted from measured  $D_{max}$  (Durand et al., 2008) was 0.09 mm for the top two layers, and was 0.28 mm for

**Table 2**

Monthly-averaged SWE from the VIC model predictions and the generic priors of snow parameters used for retrieval.

Site, Month	VIC SWE (mm)		Generic density prior ( $\text{kg}/\text{m}^3$ )		Generic snow temperature prior ( $^\circ\text{C}$ )		Generic exponential correlation length prior (mm)			
	Multi-year Average (mm)	Standard deviation between different years (mm)	Mean	Std	Mean	Std	Mean	Std		
CLPX-LSOS <sup>a</sup> Churchill	Feb	90.52	38.76		335	86	-6.5	6.5	0.18	0.18
	Jan	77.20	25.47		217	56	-10.5	10.5		
	Feb	95.79	24.41							
	Mar	108.37	25.69							
	Apr	104.59	35.78							
	Sodankylä	Nov	23.01	17.93						
	Dec	41.17	34.91							
	Jan	65.57	52.13							
	Feb	89.02	58.49							
	Mar	115.45	58.98							

<sup>a</sup> Note that the standard deviation of the generic SWE prior is 100% of the VIC SWE, which is different with the s.t.d. of VIC SWE between different years.

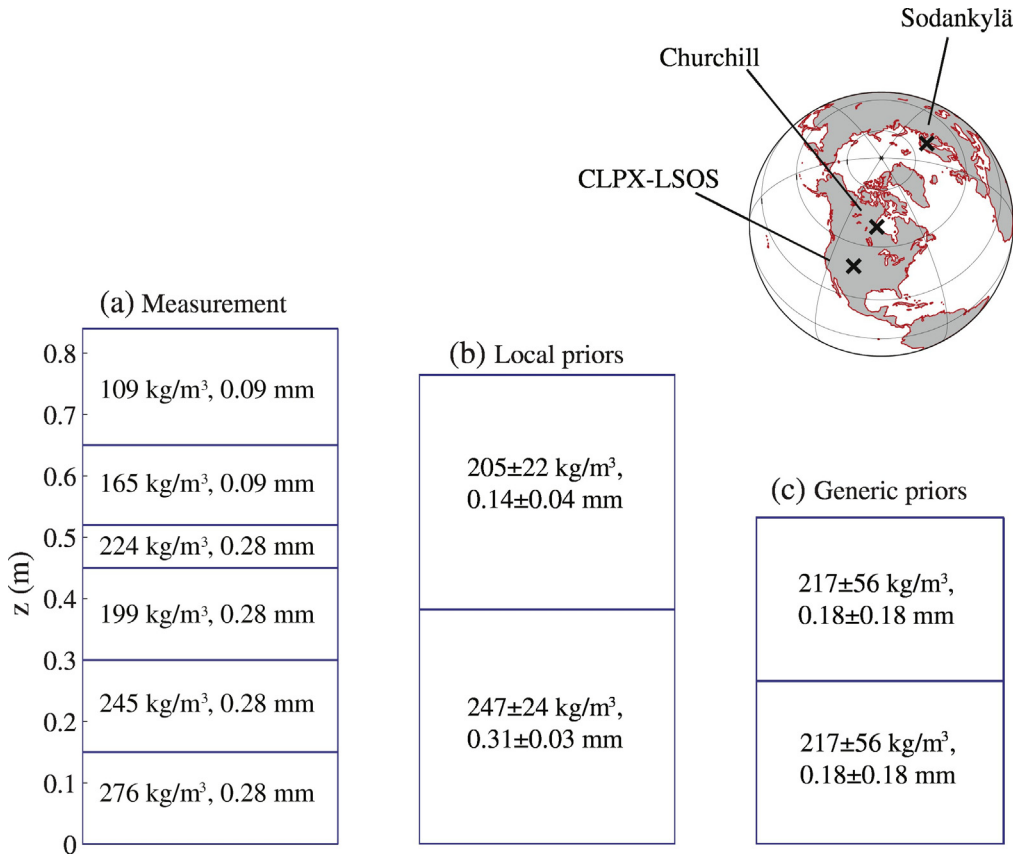


**Fig. 2.** The in-situ measurements (a) and the priors (b)–(c) for a snowpit at Sodankylä observed on March 2<sup>nd</sup>, 2010 as an example. The local priors use the average values of the measured snow properties at Sodankylä in March, see (b). The generic priors use the VIC-model SWE predictions and the Sturm's snow classes; the generic prior of  $p_{ec}$  is  $0.18 \pm 0.18$  mm, see (c). The priors for layer thickness were converted from SWE and density priors. On the up-right corner, it shows the geographic location of the sites used in this paper.

the other layers. The measured SWE is 165.9 mm. Fig. 2(b) shows the local priors using 2 layers. The local SWE prior is 173.84 mm, which is 4.7% larger than the true SWE. It was converted into slightly shallower snow depth, because the local prior of density is larger than the measured density of this snowpit. Fig. 2(c) shows the generic priors using 2 layers. The generic SWE prior is 115.45 mm, which is 30.4% smaller than the true SWE. It was converted in to a snow depth 36.7% shallower than the true depth. The prior for number of layers ( $n_{lyr}$ ) follows a Poisson distribution. In this case, the parameter  $\lambda$  of the Poisson distribution is set to 2. It means, the probability of  $n_{lyr}$  is 0.27, 0.27, 0.18, 0.09, 0.04 and 0.01 for 1, 2, up to 6 layers, respectively. This prior is used for all taiga snowpits. With this prior, the algorithm will tend to choose <3 layers.  $\lambda$  is set to 5 for alpine snowpits. The influence of the  $n_{lyr}$  prior will later be explored in the Discussion section. The prior for soil temperature was set to be the same as the prior used for the temperature of the bottom-most snow layer. The prior for soil moisture was fixed at  $8 \pm 8\%$ , and the prior for soil roughness was fixed as  $1 \pm 1$  cm, following log-normal distributions as the snow variables.

In this paper, we performed 8 experiments utilizing different choices for the SWE prior, stratigraphy prior (i.e. density, temperature,  $p_{ec}$ ) and  $T_B$ . There are two types of SWE priors: local prior from measured mean SWE, and generic prior from VIC model predictions. There are two types of stratigraphy priors: local prior from the statistics of snowpit measurements, and generic prior from snow classes. We also utilized two kinds of  $T_B$  inputted to MCMC: one is the observed (real)  $T_B$ , and the other is the synthetically generated  $T_B$  calculated by snowpit measurements with a 2-K random error added. The 8 experiments are listed in Table 3. While the focus in this paper is on estimation using real  $T_B$  data, the synthetic experiments are presented as well because we found that they shed light on understanding the performance of the algorithm.

## 6. Results

### 6.1. The performance of SWE estimation

Fig. 3 shows the performance of the SWE retrieval using BASE-PM with generic SWE and stratigraphy priors (Experiment 1), where (a) is the BASE-PM SWE versus the true SWE, and (b) is the BASE-PM estimated SWE uncertainty versus absolute SWE error. This is the result for all the 48 snowpits from Sodankylä, Churchill and CLPX-LSOS. BASE-PM SWE performance statistics are shown in Table 4, where the first row corresponds to the result in Fig. 3. For all 48 snowpits, the RMS error of estimated SWE for all snowpits is 57 mm, and the mean bias is  $-9.3$  mm. However, as shown in Fig. 3(a), there are two snowpits from the Churchill site, which have significantly higher SWE estimate than the true SWE. A Grubbs' test (Grubbs, 2007) applied on the absolute SWE error indicates these two snowpits are outliers with a significance level of 0.005. In Fig. 3(b), it shows the uncertainty estimates are also highest for these two snowpits; thus it is reflected from the retrieval algorithm that their SWE estimates are unreliable. After excluding the two outliers, the RMS

**Table 3**  
The MCMC retrieval experiments.

Experiment #	SWE prior	Stratigraphy prior	Observations
1	Generic	Generic	Real $T_B$
2	Generic	Local	Real $T_B$
3	Local	Generic	Real $T_B$
4	Local	Local	Real $T_B$
5	Generic	Generic	Synthetic $T_B$
6	Generic	Local	Synthetic $T_B$
7	Local	Generic	Synthetic $T_B$
8	Local	Local	Synthetic $T_B$

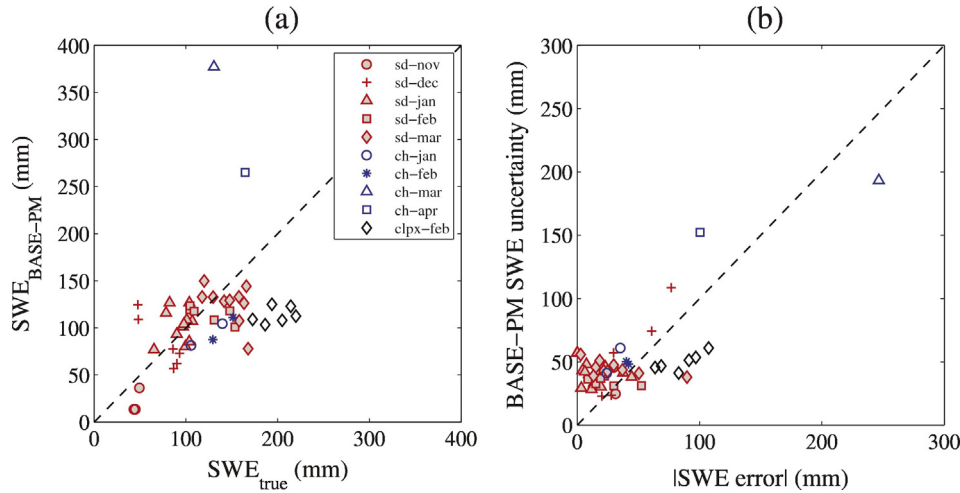


**Fig. 3.** The performance of the BASE-PM (Bayesian Algorithm for SWE Estimation-Passive Microwave) for SWE retrieval: (a) the BASE-PM SWE compared to the observed SWE at different sites and months, (b) the BASE-PM SWE uncertainty compared to the absolute SWE error. BASE-PM used the generic priors for both SWE and the snow stratigraphy feature.

error of the remaining 46 snowpits is 42.7 mm, and the mean bias is  $-17.3$  mm. They are improved compared to the RMS error (52.7 mm) and the mean bias ( $-42.1$  mm) of the generic SWE prior. In Fig. 3(a), the SWE of all CLPX snowpits are underestimated. The reason for the underestimation is most likely due to the reduced sensitivity of passive microwave signal to SWE for thick snow. Another reason could be only the  $T_B$  at three frequencies (18.7, 36.5 and 89 GHz) was measured compared to the 4-frequency  $T_B$  measurements utilized at Sodankylä (10.65, 18.7, 36.5 and 90 GHz) and Churchill (6.9, 19, 37 and 89 GHz). The frequency choice will be checked later in the synthetic experiments. If both the outliers and the CLPX snowpits are excluded, the RMS error of BASE-PM is reduced to 30.8 mm, and the mean bias is reduced to  $-7.1$  mm. In this case, our algorithm meets (or is within 0.8 mm) of the 30-mm Integrated Global Observing Strategy (IGOS) requirement for shallow snow. It should be noted that the “shallow snow” defined in IGOS is  $<300$  mm SWE, whereas the RMS error of our algorithm summarized here is for SWE  $<170$  mm (IGOS, 2007).

In Fig. 3(b), it also shows the uncertainty estimates clustered around 25–50 mm, which is indeed the precision of the method, excluding the outliers and the CLPX snowpits. The uncertainty for the CLPX snowpits is underestimated; this may be due to underestimation of the prior uncertainty. The fact that the two outlier snowpits have the highest uncertainty suggests that the BASE-PM uncertainty estimate is able to flag poor retrievals.

More results using other prior combinations can be found in Fig. 4, with statistics of their performance in Table 4. As mentioned before, the SWE RMS error using generic SWE and stratigraphy priors was 42.7 mm without outliers. In Fig. 4, the RMS error using generic SWE prior and local stratigraphy prior for the same snowpits is 33.3 mm. The RMS error using local SWE prior and generic stratigraphy prior is 29.0 mm. And, finally, the RMS error using both local priors is 28.3 mm. The statistics without CLPX snowpits is also available. Compared to when the generic priors were used, the RMS error decreased 22% (18% without the CLPX snowpits) when a better stratigraphy prior was introduced. The

RMS error decreased 32% (22% without the CLPX snowpits) when a better SWE prior was introduced. The RMS error decreased 34% (26% without the CLPX snowpits) when both a better stratigraphy prior and a better SWE were introduced. For all cases, the mean bias of SWE estimates is smaller than the local SWE prior. The RMS error of SWE estimation improves over the RMS of local SWE prior when the outlier snowpits and the CLPX snowpits are excluded. Thus, prior information on either SWE or stratigraphy improves the BASE-PM SWE estimation performance.

## 6.2. Results of synthetic test

Fig. 5 shows the retrieved SWE using the synthetic  $T_B$ , and the statistics is shown in Table 5. First, In contrast with the results using real  $T_B$ , the SWE outliers for these two Churchill snowpits are no longer found. The SWE RMS error and bias become similar with or without these two snowpits. Therefore, it shows the outliers may be related to some special features in the snowpack or the soil, or a limitation of the microwave model, and thus was not reflected in the synthetic  $T_B$ . The underestimations for the CLPX snowpits were reproduced by the synthetic test. Also, it shows that the underestimation is not related to the frequency choice, because the results using 4-frequency synthetic  $T_B$  with an additional frequency as 10.65 GHz (in black stars) are not significantly better than the results using 3-frequency synthetic  $T_B$  (in black diamonds).

In the synthetic test, the RMS SWE error is also smaller when the more accurate local SWE or stratigraphy prior than the generic priors is used. It supports the conclusions found in Section 6.1 using real  $T_B$ : using more accurate priors, where available, can improve the accuracy of SWE retrieval.

## 6.3. Markov chains of snow and soil variables

This section shows more details of the BASE-PM algorithm when it was applied on the example snowpit mentioned in Section 5, Fig. 2.

**Table 4**  
Error of MCMC-retrieved SWE using observed  $T_B$ .

	Experiment #	SWE prior	Stratigraphy prior	All snowpits		Excluding two pits at Churchill		Excluding two pits at Churchill, and CLPX snowpits	
				RMS error (mm)	Mean bias (mm)	RMS error (mm)	Mean bias (mm)	RMS error (mm)	Mean bias (mm)
Retrieved SWE	1	Generic	Generic	57.0	$-9.3$	42.7	$-17.3$	30.8	$-7.1$
	2	Generic	Local	64.2	3.7	33.3	$-7.6$	25.2	0.8
	3	Local	Generic	34.1	$-0.04$	29.0	$-3.7$	24.1	3.0
	4	Local	Local	36.0	2.0	28.3	$-2.5$	22.8	4.6
Prior SWE	Generic SWE prior		52.3		$-42.0$	52.7	$-42.1$	36.9	$-32.2$
	Local SWE prior		25.5		11.7	24.9	11.5	25.4	15.3

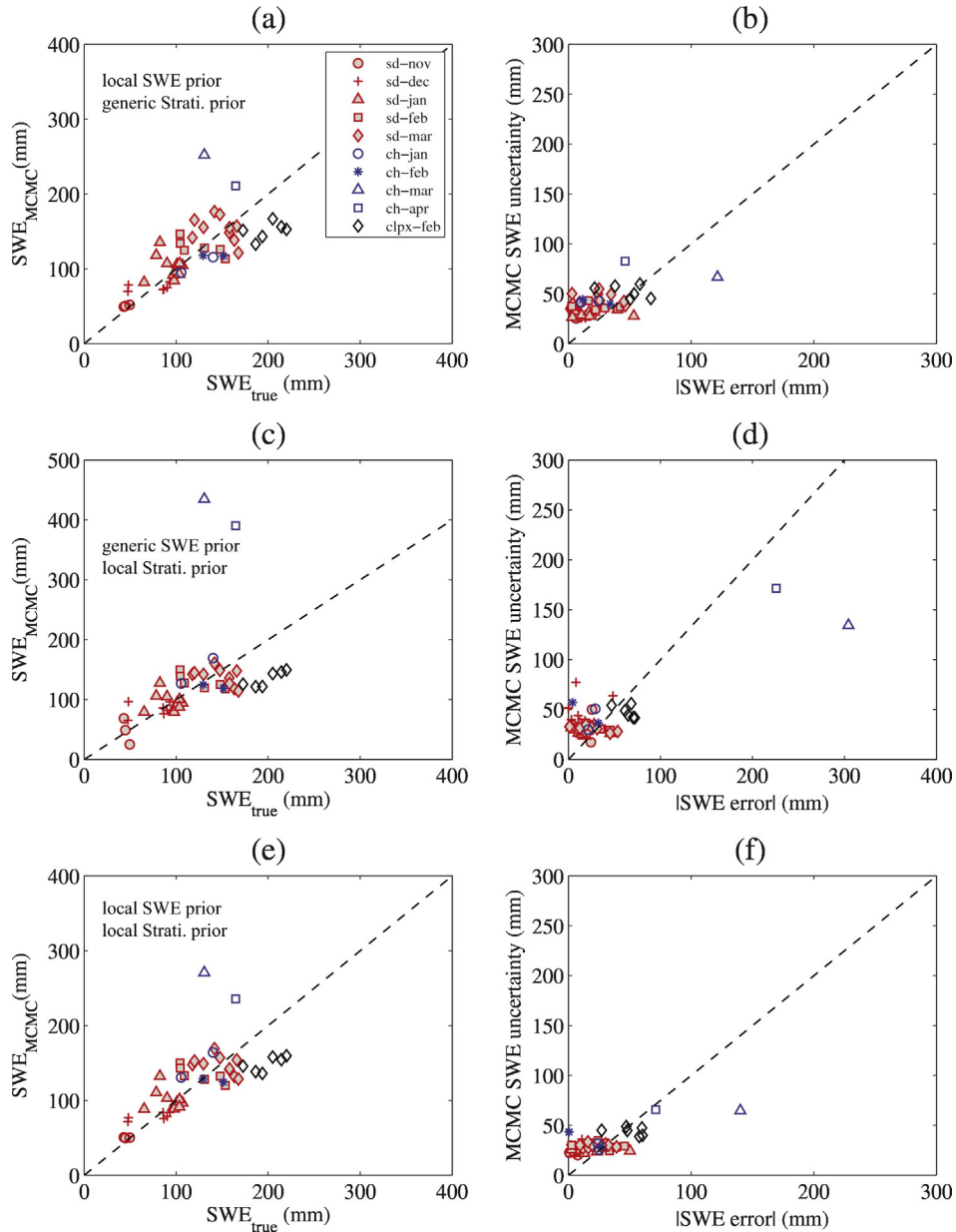


**Fig. 4.** The MCMC-estimated SWE compared to the observed SWE using observed  $T_B$  from radiometers, when (a) local SWE prior but generic stratigraphy (Strati.) prior were used; (c) generic SWE prior but local stratigraphy prior were used; (e) local SWE prior and local stratigraphy prior were used. In (b), (d) and (f), it shows the MCMC SWE uncertainty versus the absolute SWE error, corresponding to (a), (c) and (e), respectively.

Fig. 6 shows the Markov chains of the snow layer thickness, density,  $p_{ec}$  and temperature when the generic SWE prior and stratigraphy prior were used. The chains randomly jumped within a large range for each variable after adjusted during the burn-in period. For example, in the first 2000 iterations of the burn-in period, the  $p_{ec}$  of the bottom layer increases from the prior value as 0.18 mm to above 0.3 mm. Then, it randomly fluctuates between 0.25 and 0.5 mm with a stable standard deviation. Using the values of variables at each iteration, a corresponding  $T_B$  chain can be calculated, as shown in Fig. 7. The RMS error of the  $T_B$  chain compared to the observed  $T_B$  is 2.19 K, 4.17 K, 2.07 K and 2.17 K at 10.65, 18.7, 36.5 and 89 GHz. The RMS error at 18.7 GHz is larger because the mean bias ( $-3.98$  K) at this frequency is also larger than other frequencies (1.38 K, 0.76 K and  $-0.79$  K at 10.65, 36.5 and 89 GHz, respectively). This may be due to some physical emission characteristics at 18.7 GHz that are not well-represented by the observation model. Note that many other snowpits have a good (RMS error smaller

than 2.0 K)  $T_B$  chain at 18.7 GHz, too. The standard deviation of the  $T_B$  chains all fall below 2 K for the four frequencies (1.71 K, 1.27 K, 1.93 K and 2.02 K at 10.65, 18.7, 36.5 and 89 GHz, respectively). This indicates that many combinations of snow/soil properties could produce a similar  $T_B$  signal. However, if a SWE chain is produced using the layered snow thickness and density from these combinations, it could be found in Fig. 8 that, the SWE chain basically follows a log-normal distribution. The uni-modal shape of the SWE chain indicates that there are some SWE values which have a higher probability than other values. This is because the MCMC algorithm sampled the combinations of snow variables conditioned on the  $T_B$  observations. For the snowpit example here, the retrieved SWE is 144.3 mm with an estimated uncertainty of 42.9 mm. The true SWE is 165.9 mm, and thus the absolute error is 21.6 mm. The retrieved SWE is more accurate than the prior SWE estimate (115.45 mm).

Fig. 9 is the histogram of the snow variables (snow layer thickness, density, temperature and  $p_{ec}$ ). The posterior distributions of these

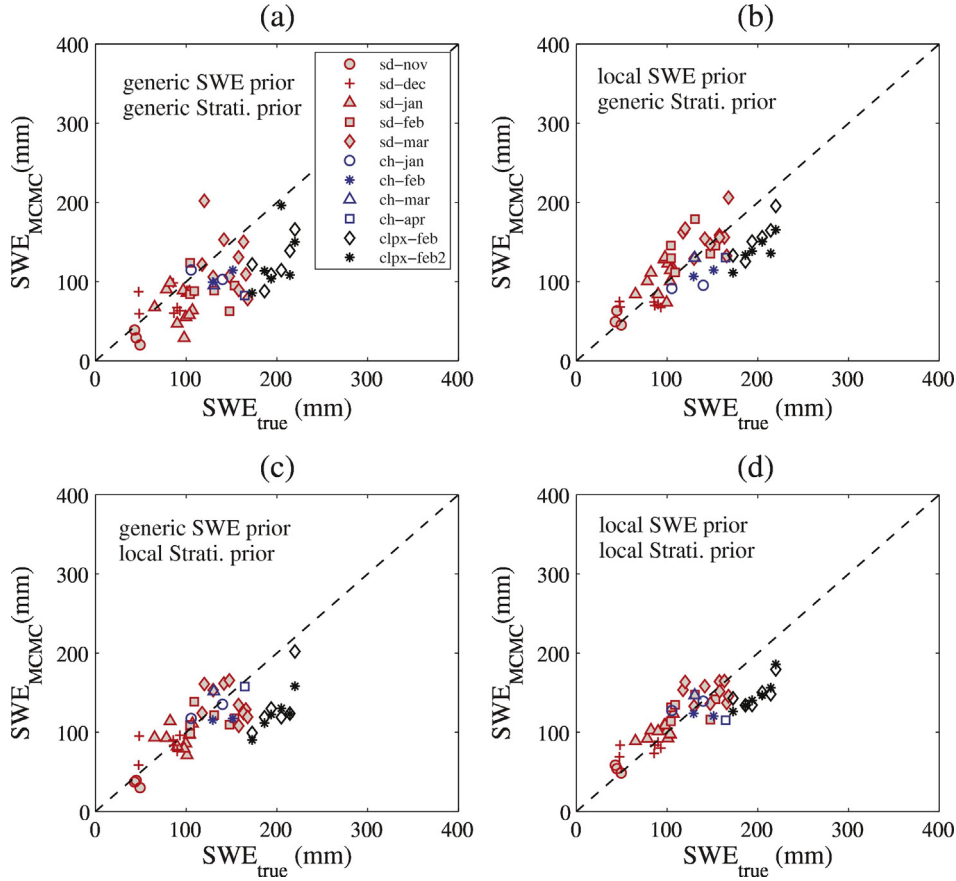


**Fig. 5.** The MCMC-estimated SWE compared to the observed SWE using synthetic  $T_B$ , when (a) generic SWE prior and generic stratigraphy (Strati.) prior were used; (b) local SWE prior but generic stratigraphy prior were used; (c) generic SWE prior but local stratigraphy prior were used; (d) local SWE prior and local stratigraphy prior were used.

variables are also uni-modal. Table 6 summarizes the retrieved values for all snow and soil properties. The “true” 2-layer thickness, density, temperature and  $p_{ec}$  shown here are derived from the measured snow properties using the re-layering approach mentioned before. The retrieved snow depth is 0.69 m, which is 17.9% shallower than the true snow depth, but the retrieved layer thicknesses are quite different from the measurement re-layered values. Thus, snow property estimates for individual layers are generally less accurate than bulk estimates. For example, it is also very interesting to find that the overall SWE accuracy is better than the accuracy of layer thickness or the density for specific layers. The retrieved layer thickness is 50.0% lower at the bottom layer and 25% higher than the surface layer; and, the retrieved density is 0.5% higher for the bottom layer and 37.7% higher for the surface layer. On the contrary, the retrieved SWE is only 13.1% less than the true SWE. However, the algorithm successfully estimated a lower  $p_{ec}$  at the surface layer than the bottom layer, when 0.18 mm  $p_{ec}$  prior was used for both layers. The reason for the less accurate snow properties at specific layers is most likely due to the lack of enough prior information to constrain the estimates. Of all the snow variables, the sensitivity of passive microwave  $T_B$  to density and temperature is small. To match

the  $T_B$  measurements, the layer thickness and  $p_{ec}$  are most important, and their estimates can largely compensate for the effects in density and temperature estimates. However, there are still many combinations of layered thickness and  $p_{ec}$  that can give similar  $T_B$  signals. For example, as shown in Fig. 6(a) and (c), the thickness of the bottom layer shows a negative correlation with the  $p_{ec}$  of the bottom layer. The relatively large  $p_{ec}$  at the bottom layer in Fig. 6(c) corresponds to the relatively smaller thickness of the bottom layer. These two parameters compensate for each other. This highlights the importance of the histogram of posterior SWE; the histogram provides the uncertainty embedded in the uncertainty of all snow parameters that can influence the SWE estimation.

For soil parameters, the soil temperature was estimated with a relative bias of  $-1.4\%$ . The estimated soil roughness is 0.7 cm, which is close to the soil roughness measured by gridded reference panel (0.8 cm). Use of a no-snow  $T_B$  measurement, if available, could potentially help to determine soil roughness, in some cases; this will be explored in future work. The estimated soil moisture is quite different than the measurement. This is because the sensitivity of  $T_B$  to soil moisture reduces quickly for large soil roughness and frozen soil.

**Table 5**  
Error of MCMC-retrieved SWE using synthetic  $T_B$ .

Experiment #	SWE prior choice	Stratigraphy prior choice	All snowpits		Excluding two pits at Churchill		Excluding two pits at Churchill, and CLPX snowpits		
			RMS error (mm)	Bias (mm)	RMS error (mm)	Bias (mm)	RMS error (mm)	Bias (mm)	
Retrieved SWE	5	Generic	Generic	47.6	-29.5	46.7	-28.2	39.9	-21.1
	6	Generic	Local	33.9	-12.0	34.5	-12.8	24.5	-4.7
	7	Local	Generic	28.4	-1.9	28.6	-1.2	24.8	5.3
	8	Local	Local	26.4	-2.9	25.8	-2.3	18.8	4.9

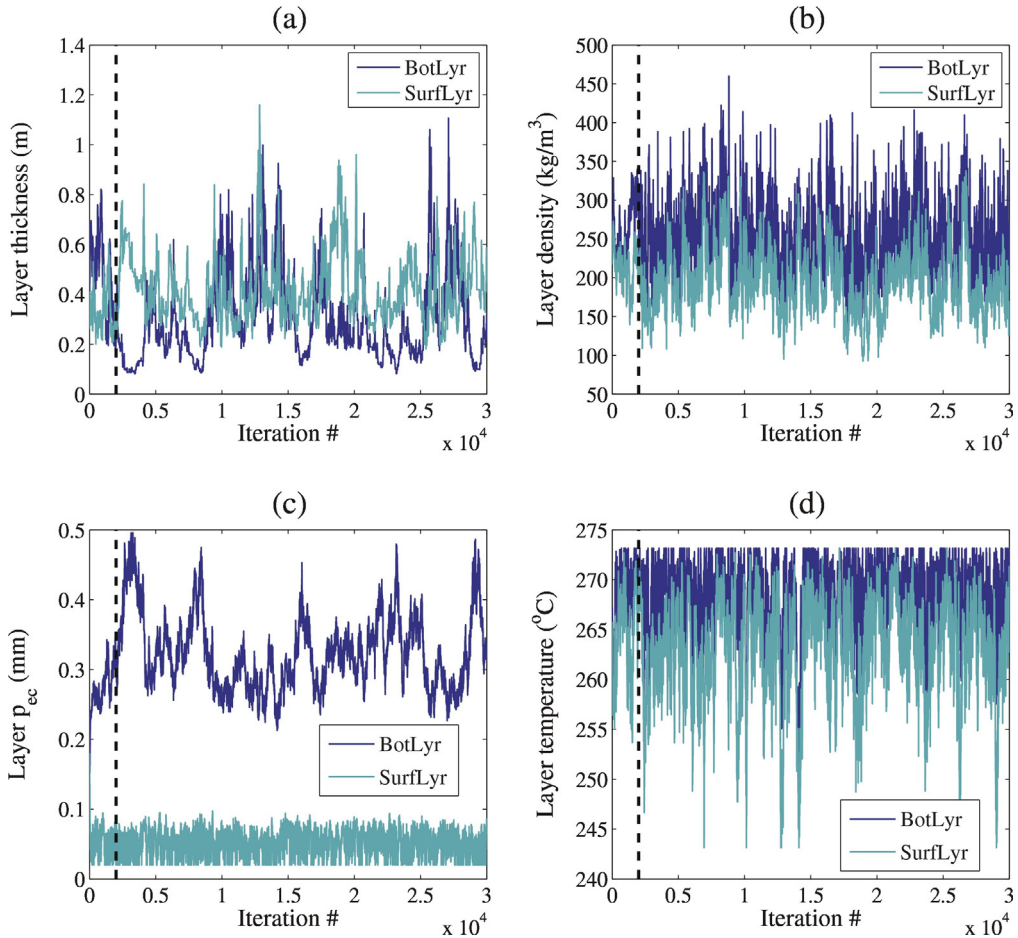


**Fig. 6.** The BASE-PM Markov chains of the snowpit observed at Sodankylä on March 2<sup>nd</sup>, 2010 for (a) snow layer thickness, (b) snow density, (c)  $p_{ec}$  and (d) temperature, when generic SWE and stratigraphy priors were used. BASE-PM chose 2 layers, where "BotLyr" is for the chain of the bottom layer, and "SurfLyr" is for the chain of the surface layer.

## 7. Discussion

### 7.1. Analysis of the response of microwave $T_B$ to SWE

To better understand the reason for the outliers and the underestimation for the CLPX snowpits, we plotted the measured (real) and the synthetic  $T_B$  versus SWE for all the 48 snowpits at different frequencies.

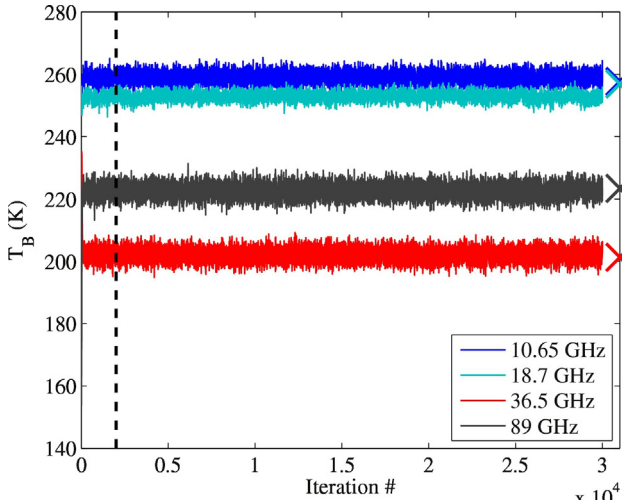


**Fig. 7.** Simulated  $T_B$  from the estimated snow and soil variables in Fig. 6, where the crosses are the measured  $T_B$  at four frequencies.

As shown in Fig. 10, both the measured  $T_B$  and the synthetic  $T_B$  at 36.5 GHz show a decreasing trend as the SWE increases from 40 mm to about 120 mm. This trend becomes unclear for  $SWE > 120$  mm due to the influence of other snow parameters. This explains why the underestimation for CLPX snowpits can happen because their SWE is inside

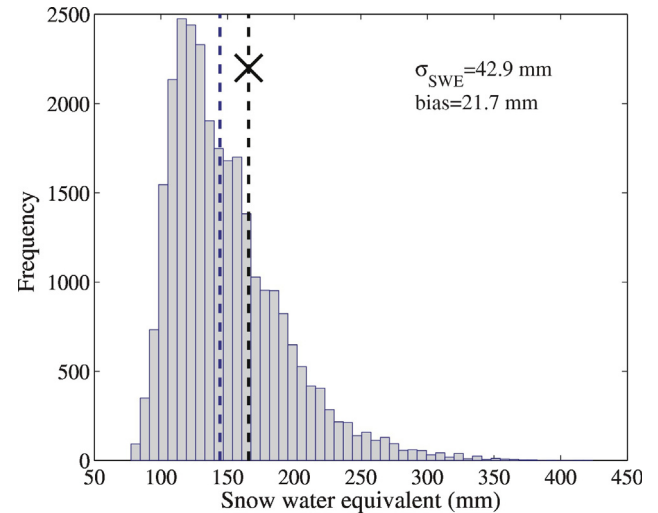


**Fig. 8.** Histogram of the SWE chain for the example Sodankylä snowpit, where the blue dash line indicates the BASE-PM SWE, and the black dash line indicates the measured SWE. (For interpretation of the references to colour in this figure legend, the reader is referred to the web version of this article.)

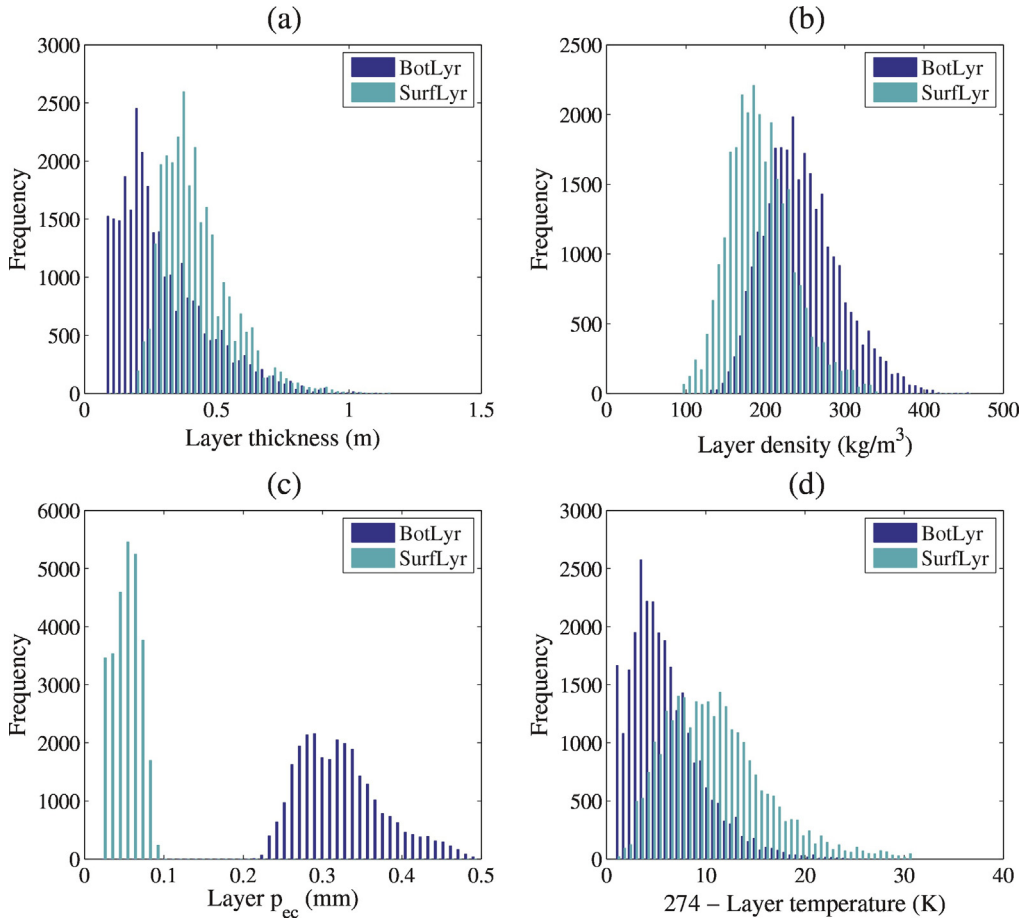


**Fig. 9.** Histogram of the chains in Fig. 6 after the burn-in period for: (a) layer thickness, (b) density (b), (c)  $p_{ec}$ , and (d) 274 K minus snow temperature in K. In (d), the variable estimated related to temperature is 274 K minus the temperature in K, because the assumption of a log-normal distribution requires positive values.

this insensitive region. More information can be found in simulation test results in Fig. 11, where the measured multiple-layer snow density, temperature and  $p_{ec}$  were used for simulation for each snowpit, but the total snow depth was scaled to match the different SWE in X-axis. Each line corresponds to a snowpit, and the relative thickness of layers was not changed. In general, it shows that, the simulated  $T_B$  at 36.5 GHz decreases with the increasing SWE from 20 mm up to about 160 mm. After 160 mm, the simulated  $T_B$  begins to increase with increasing SWE, for some snowpits. This trend is also found in the field measurements for tundra snow in Canada (Derksen et al., 2010) and

alpine snow in Switzerland (Matzler et al., 1982). The inflection point from decreasing to increasing trend is determined by snow properties, especially, the snow micro-structure parameter. This complex  $T_B$  response indicates that it can be hard to do SWE retrieval for deep snow, unless we have better information of other related snow properties.

Another interesting thing is the sensitivity of 89-GHz  $T_B$  to SWE, as can be found both in measurements (Fig. 10(a)) and simulations (Fig. 10(b) and Fig. 11). The reason for the sensitivity will be discussed later in the next subsection. For some snowpits, the 89-GHz  $T_B$  is sensitive to SWE when the 36.5-GHz  $T_B$  is not. It indicates the inclusion of this frequency may help improve the SWE retrieval if it is used properly.

For the lower frequencies, the results based on the both measured and synthetic  $T_B$  in Fig. 10 show that  $T_B$  at 6.925 and 10.65 GHz is insensitive to SWE. This is because, according to RT theory, the dimension of snow particles is much smaller than the long wavelength at such frequencies, and the volume scattering effect is weak; these channels may aid in estimation of soil properties. In Fig. 10(a), there are two snowpits with the measured  $T_B$  at 18.7 GHz lower than 240 K, which is not found for snowpits with similar SWE or in their corresponding synthetically generated  $T_B$  in Fig. 10(b). These are the two Churchill snowpits where the strongly overestimated BASE-PM SWE was produced. Fig. 11 demonstrates why such overestimation is possible, because in general, with long wavelength,  $T_B$  at 18.7 GHz is only slightly sensitive to SWE for shallow snow; this sensitivity becomes more apparent only for very deep snow. According to our tests (not shown here), the very low  $T_B$  at 18.7 GHz but not 10.65 GHz may be related to the coherent effects of ice lenses with some specific thicknesses. It indicates, although 18.7-GHz remains sensitive for deep snow, other factors which also have influence needs to be considered. For these two

**Table 6**

The estimated snow and soil parameters for the example Sodankylä snowpit observed on March 2<sup>nd</sup>, 2010 when generic SWE and stratigraphy priors were used.

Estimated variables	MCMC retrieval	True values <sup>a</sup>
Snow layer thickness	Bottom layer	0.26
	Surface layer	0.32
Snow density	Bottom layer	242.85
	Surface layer	189.56
$p_{ec}$	Bottom layer	0.320
	Surface layer	0.051
Snow temperature	Bottom layer	-4.4
	Surface layer	-8.9
Snow depth		0.69
Snow water equivalent		144.2
Soil temperature		-4.21
Soil moisture (%)		7.01
Soil roughness (cm)		0.702

<sup>a</sup> The true values of the snow variables were re-layered from the original 6-layer measurements.

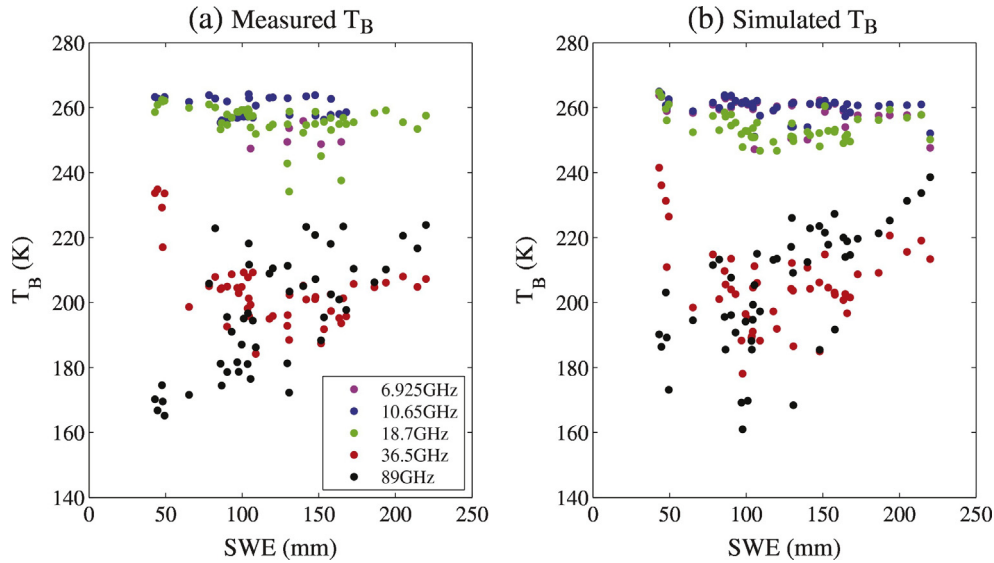


**Fig. 10.**  $T_B$  at 6.925 to 89 GHz versus SWE for all the 48 snowpits, where in (a) it shows the measured  $T_B$ , in (b) it shows the synthetic  $T_B$ .

snowpits, the retrieved SWE can be improved by excluding this frequency.

#### 7.2. The influence of the number of snow layers

The issues related to the number of snow layers ( $n_{lyr}$ ) can be summarized in the following three questions: first, how many snow layers does the snowpit truly have? Second, how many snow layers are required to reproduce the measured  $T_B$  signal? Finally, will the prior for the number of snow layers influence the retrieved SWE?

The natural snow cover is vertically-inhomogeneous and could have many layers. For the Sodankylä snowpits, usually 5 to 10 layers were recorded. The Churchill snowpits measured by the Environment Canada group had 4 to 7 layers. The most high-frequent number of layers is two for the entire CLPX study region (Durand and Liu, 2012), and five for the Fraser MSA.

In this study, due to the computational cost, we ran BASE-PM with a maximum of 6 layers. In most cases, the algorithm chose 2 layers. Using the generic prior, more layers were not chosen, because it was found that the observed  $T_B$  at all frequencies utilized in this paper can be

reproduced well by a 2-layer profile. On the other hand, it was found at least two layers were required for some snowpits to match the  $T_B$  observations, especially when the measured  $T_B$  at 89 GHz is higher than 36.5 GHz. Fig. 12 shows the SWE estimates when BASE-PM was forced to choose 1 layer. The RMS error of SWE is 79.2 mm for all snowpits, and 73.2 mm excluding the two Churchill snowpits. For true SWE between 90 and 250 mm, the estimated SWE for most snowpits is between 160 and 190 mm. Moreover, the uncertainty of the SWE estimates is dramatically underestimated. Presumably, this is because constraining the snowpack to a single layer essentially presupposes a simpler radiative transfer dynamic that does not hold, for these snowpits.

To understand the reasons, Fig. 13(a) shows the simulated  $T_B$  versus SWE for all snowpits like in Fig. 12, but the simulations here used mass-weighted (1-layer) snow properties in the first row, and 2-layer snow properties (re-layered from the original snowpit measurements) in the second row. It shows when snow has only 1-layer, the simulated  $T_B$  at 89 GHz will not change when SWE is larger than 40 mm. However, it conflicts with the true SWE- $T_B$  relationship according to measurements in Fig. 10(a) and simulations using originally-measured multiple-layer snow profiles in Fig. 11. The increasing trend of 89-GHz  $T_B$  with SWE

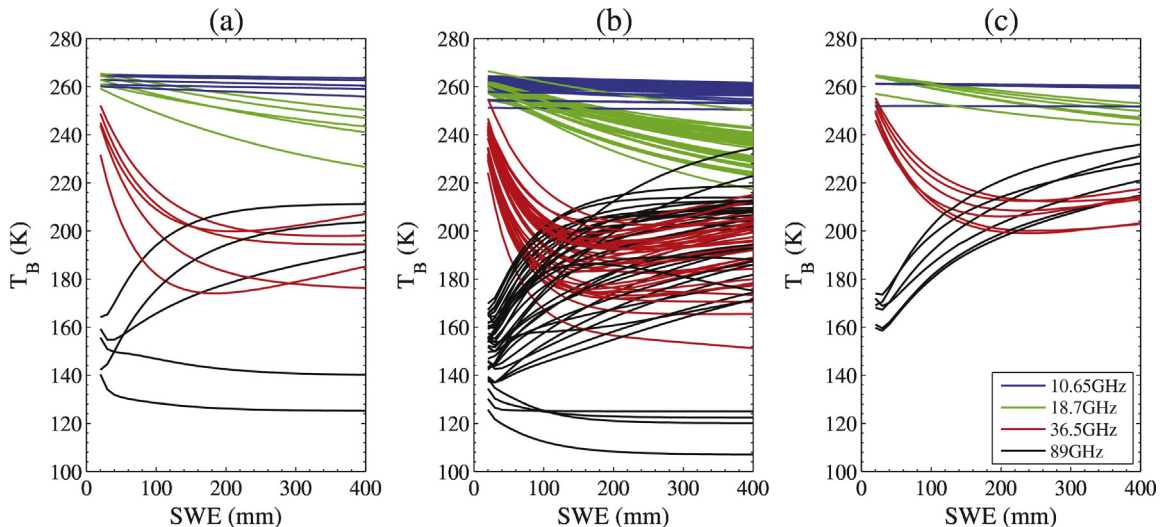


**Fig. 11.** Simulated  $T_B$  at 10.65 to 89 GHz using the measured snow density, temperature and  $p_{ec}$  for each snowpit but the snow depth was scaled to match the SWE from 20 mm to 400 mm in X-axis. Each line corresponds to the  $T_B$ -SWE relationship for one snowpit at one frequency: (a) for the snowpits with SWE between 40 and 50 mm; (b) for the snowpits with SWE between 50 and 170 mm; (c) for the snowpits with SWE larger than 170 mm (i.e. the CLPX snowpits).

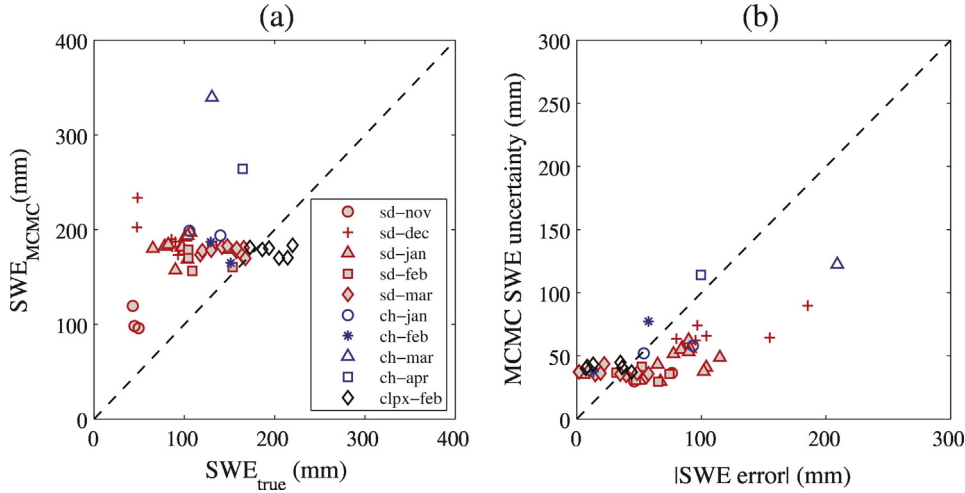


**Fig. 12.** The SWE using 1-layer snow parameter estimation when the same priors as BASE-PM were used: (a) the MCMC SWE versus the true SWE; (b) the estimated SWE uncertainty versus the absolute SWE error.

can be reproduced using 2-layer snow. The reason for the sensitivity of 89-GHz to SWE is related to stratigraphy. Fig. 14 shows the upward-propagated  $T_B$  at 89 GHz inside snowpack using the method in Pan et al. (2016) when the 6-layer (originally-measured), 2-layer and 1-layer snow profiles are used for the example snowpit mentioned in Section 5. This snowpit has two surface layers with a  $p_{ec}$  of 0.09 mm and a density smaller than 200 kg/m<sup>3</sup>. Fig. 14 shows that the decrease of upward-propagated  $T_B$  is slower in the surface layers than the bottom layers. The changing rate of upward-propagated  $T_B$  is more influenced by  $p_{ec}$  than density. When there is only 1 layer, no matter if the snow depth is 84 cm, or 2/3 or 1/3 of the original depth,  $T_B$  decreases to the same value as about 142 K at the snow surface. However, when there are at least two layers, the snow profile with thicker snow depth has thicker surface layer with small scattering, and according to RT theory, the snow-emitted  $T_B$  in this layer increases the  $T_B$  observed at the snow surface. The simulation here assumed unchanged relative thickness of layers. However, if we fixed the density and thickness of the surface layer and scaled only the thickness of the bottom layer to match 2/3 or 1/3 SWE, we will have again similar  $T_B$  (200.8 K) as the original snow profile. Therefore, it indicates that the increase in 89-GHz  $T_B$  with increasing SWE is related to the thickness of the surface layer with smaller  $p_{ec}$ . In natural conditions, snow compaction and grain growth are gradual and continuous processes throughout the entire snowpack. It is hard to keep the thickness of surface low- $p_{ec}$  layer unchanged, but increasing only the SWE amount in the bottom layers. Therefore, sensitivity of 89-GHz  $T_B$  is partly related to the snow emission theory, but also influenced by the natural properties of snow. Additionally, related to the effects of layered snow, note that  $T_B$  at 36.5 GHz will increase with increasing SWE when SWE is larger than a certain value using the measured snow profiles, but this feature can also not be captured by a 1-layer model. Therefore, considering at least two snow layers is important for passive microwave SWE estimation, especially for deep snow case.

To test the influence of the prior for number of snow layers ( $n_{lyr}$ ), we tried different  $\lambda$  for Poisson distribution, or different types of prior distributions (for example, a uniform distribution). Results show that the algorithm continued to choose 2 layers as long as generic stratigraphy prior was used. When local stratigraphy prior was used, more layers may be chosen for some snowpits, but the resulted change in SWE for these snowpits was only between 2 and 8 mm. Therefore, in general, the prior for  $n_{lyr}$  is not important.

### 7.3. Length of the Markov chain

When the MCMC algorithm was utilized, at each iteration, it samples a combination of estimated variables which could reproduce the  $T_B$

observation from the prior distribution. The Markov chain built by these combinations will become gradually stable when the sample size is sufficiently large. Therefore, for reasons of computational efficiency, it is important to check how many iterations are required to give a stable output.

One way to find the required chain length is to track the changes in the mean and the standard deviation of the chain. When a chain becomes stable, the mean and the standard deviation of the chain after the burn-in period will not change strongly when additional iterations are performed. For the example Sodankylä snowpit, our test shows the change of mean and standard deviation of the chain between two subsequent iterations dropped below 5% at the 18,000-th iteration, and below 3% at the 20,800-th iteration.

Another way is to check the convergence of the chains if they are started from different initial values (Gelman et al., 1995). Usually the Markov chains in our paper start from  $\exp(\mu_{logx} + 0.5\sigma_{logx}^2)$  for all variables. Here four additional scenarios are considered to perform a test, where the initial values are (1)  $\exp(\mu_{logx} + 2\sigma_{logx}^2)$  for all variables; (2)  $\exp(\mu_{logx} - \sigma_{logx}^2)$  for all variables; (3)  $\exp(\mu_{logx} + 2\log x\sigma_{logx}^2)$  for layer thickness, and  $\exp(\mu_{logx} + 0.5\sigma_{logx}^2)$  for other variables; (4)  $\exp(\mu_{logx} - \sigma_{logx}^2)$  for layer thickness, and (5)  $\exp(\mu_{logx} + 0.5\sigma_{logx}^2)$  for other variables. A between-chain variance ( $B$ ) and a within-chain variance ( $W$ ) are calculated from these five chains, as can be found in Gelman et al. (1995). Later, an index  $\sqrt{\bar{R}}$  is used to compare the difference between  $B$  and  $W$ :

$$\sqrt{\bar{R}} = \sqrt{\frac{n-1}{n}W + \frac{1}{n}\bar{B}} \quad (12)$$

where,  $n$  is the length of the chains. In theory,  $\sqrt{\bar{R}}$  is larger than 1, but it decreases to 1 as  $n$  approaches infinity. When  $\sqrt{\bar{R}}$  is smaller than 1.2, it means  $B$  is comparable to  $W$ , and the chains are considered to have converged (Gelman et al., 1995). In our test,  $\sqrt{\bar{R}}$  became smaller than 1.2 at the 4365-th iteration, and became smaller than 1.02 at the 25,600-th iteration. Combined together with the previous test, we concluded a number of 20,000 iterations are enough for SWE retrieval. This is before any advanced MCMC approaches are used (Roberts and Rosenthal, 2009; Yardim et al., 2006). Fig. 15 shows the first 5000 iterations of the five scenarios. It shows the different chains quickly merged to similar SWE values before the 2000-th iteration. Therefore, a burn-in period of 2000 iterations used in this paper is also appropriate.

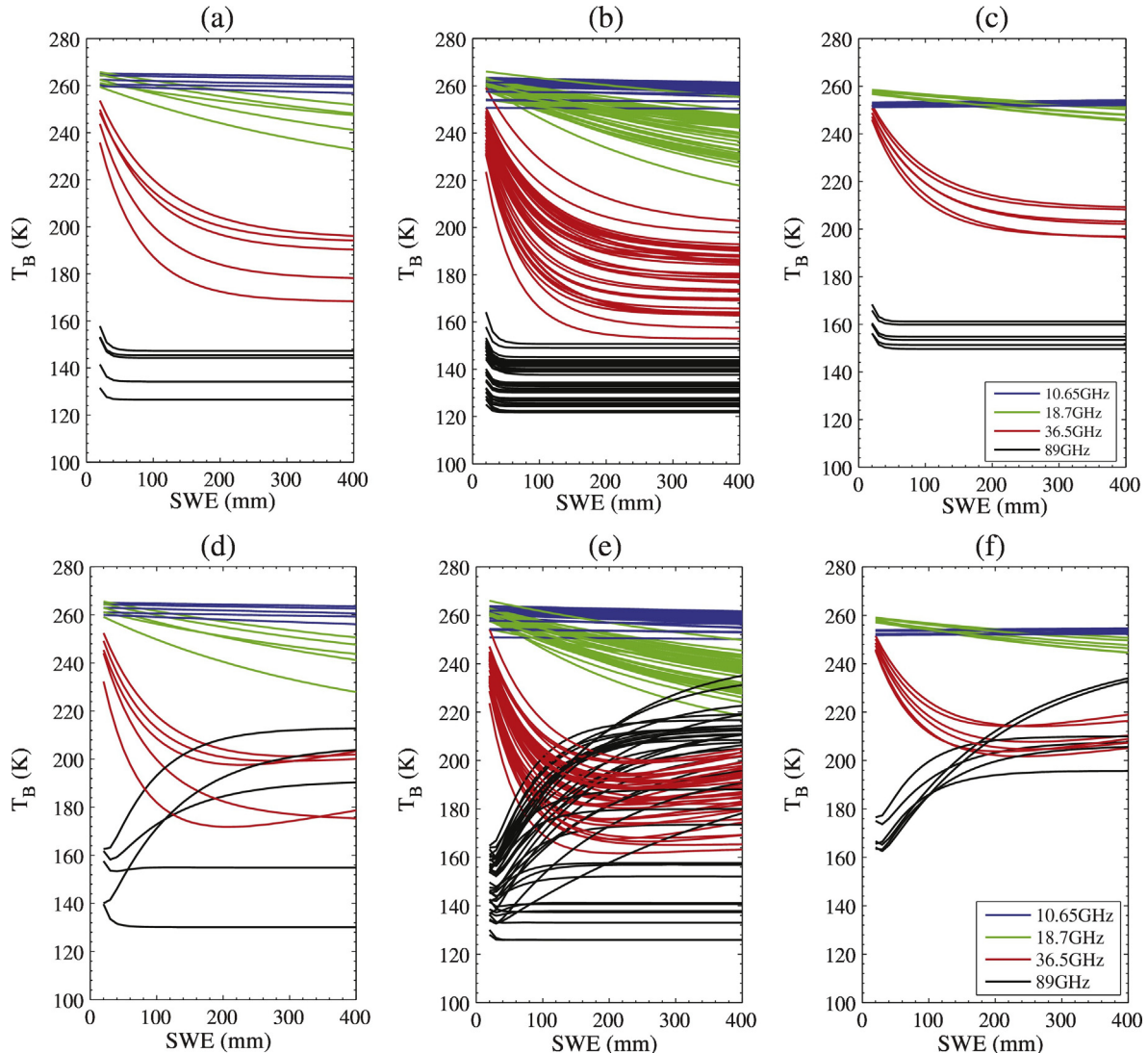


**Fig. 13.** Simulated  $T_B$  at 10.65 to 89 GHz using the 1-layer (first row) or 2-layer (second row) snow density, temperature and  $p_{ec}$  for each snowpit, where the snow depth was scaled to match the SWE from 20 mm to 400 mm in X-axis. Each line corresponds to the  $T_B$ -SWE relationship for one snowpit at one frequency. From left to right: the first column is for the snowpits with SWE between 40 and 50 mm; the second column is for the snowpits with SWE between 50 and 170 mm; the third column is for the snowpits with SWE larger than 170 mm (i.e. the CLPX snowpits).

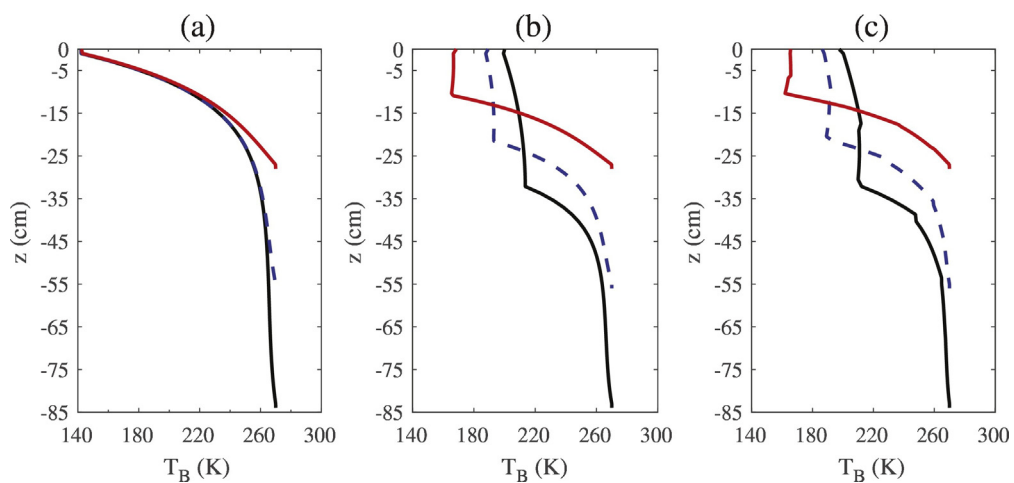


**Fig. 14.** Simulated upward propagated  $T_B$  at 89 GHz, vertical polarization for the example snowpit. From left to right, we used 1-layer, 2-layer and 6-layer snow profiles. The originally-measured snow depth was used for the black line; for blue dash line and red line, the snow depth was scaled by 2/3 and 1/3, respectively, with relative thickness of layers unchanged. (For interpretation of the references to colour in this figure legend, the reader is referred to the web version of this article.)

## 8. Conclusions

The BASE-PM algorithm presented herein has been shown to accurately retrieve SWE from ground-based  $T_B$  observations, with an RMS error of 30.8 mm (excluding deeper snow and two outliers), which meets the requirements of Integrated Global Observing Strategy (IGOS) for shallow snow. This algorithm is applicable globally, requiring only globally-available prior information; next steps should include testing on a larger dataset, and utilizing with airborne and spaceborne  $T_B$  measurements.

The algorithm did not perform well for the CLPX-LSOS snowpits with SWE larger than 170 mm. An underestimation was found for these deep snowpits, and this effect was reproduced by the synthetic experiments. There were also two outliers, where the algorithm gave abnormally large SWE estimation. The uncertainty estimation gave a large uncertainty for these two snowpits, as well. The outliers were not present in the synthetic test. According to the analysis, this is most likely due to the low measured  $T_B$  at 18.7 GHz with the unknown effect not recorded by the snowpit measurement.

The benefit of the Bayesian based SWE retrieval algorithm is that it can incorporate the measurements from different sources as long as the signal can be simulated and reproduced by observation models. Therefore, the framework could be easily expanded to other snowpits or other radiometric measurements. The SWE uncertainty estimated by this algorithm could help recognize outliers when the true SWE is not available. This uncertainty estimate will be helpful when the SWE result is merged with the estimation from other techniques.

## Acknowledgment

This work is supported by funds from the China Scholarship Council (2012–2016) and the NASA New Investigator Program (NNX13AB63G).

The authors want to acknowledge NASA (National Aeronautics and Space Administration) for supporting the Cold Land Processes Field Experiment (CLPX), the Canadian Space Agency for supporting the Canadian CoReH<sub>2</sub>O Snow and Ice Experiment, and the European Space Agency for supporting the Nordic Snow Radar (NoSREx) Experiments. We want to thank all the great researchers and organizers who putted their efforts and participated in these great and successful experiments, and collected valuable legacy data to be used for the entire community.

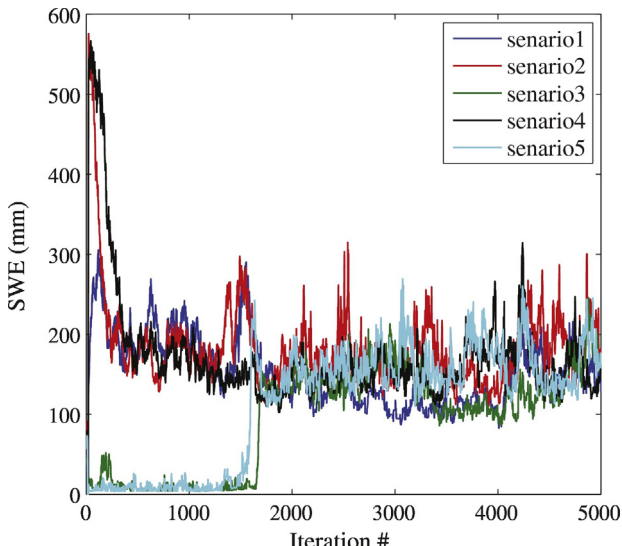


**Fig. 15.** SWE chains of the five scenarios using different initial values.

## References

- Andreadis, K.M., Lettenmaier, D.P., 2012. Implications of representing snowpack stratigraphy for the assimilation of passive microwave satellite observations. *J. Hydrometeorol.* 13:1493–1506. <http://dx.doi.org/10.1175/JHM-D-11-0561.1>.
- Armstrong, R.L., Chang, A., Rango, A., Josberger, E., 1993. Snow depths and grain-size relationships with relevance for passive microwave studies. *Ann. Glaciol.* 17, 171–176.
- Butt, M.J., 2009. A comparative study of Chang and HUT models for UK snow depth retrieval. *Int. J. Remote Sens.* 30 (24):6361–6379. <http://dx.doi.org/10.1080/01431160902852804>.
- Butt, M.J., Kelly, R.E.J., 2008. Estimation of snow depth in the UK using the HUT snow emission model. *Int. J. Remote Sens.* 29 (14):4249–4267. <http://dx.doi.org/10.1080/01431160801891754>.
- Chang, A.T.C., Foster, J.L., Hall, D.K., 1987. Nimbus-7 SMMR derived global snow cover parameters. *Ann. Glaciol.* 9, 39–44.
- Clifford, D., 2010. Global estimates of snow water equivalent from passive microwave instruments: history, challenges and future developments. *Int. J. Remote Sens.* 31 (14): 3707–3726. <http://dx.doi.org/10.1080/01431161.2010.483482>.
- Cline, D., Armstrong, R., Davis, R., Elder, K., Liston, G., 2003. CLPX LSOS snow pit measurements. In: Parsons, M., Brodzik, M.J. (Eds.), In CLPX-Ground: Snow Measurements at the Local Scale Observation Site (LSOS), J. Hardy, J. Pomeroy, T. Link, D. Marks, D. Cline, K. Elder, R. Davis. 2003. NASA DAAC at the National Snow and Ice Data Center, Boulder, CO Updated July 2004.
- Davis, D.T., Chen, Z., Tsang, L., Hwang, J.N., Chang, A.T.C., 1993. Retrieval of snow parameters by iterative inversion of a neural network. *IEEE Trans. Geosci. Remote Sens.* 31:842–852. <http://dx.doi.org/10.1109/36.239907>.
- Derksen, C., Toose, P., Rees, A., Wang, L., English, M., Walker, A., Sturm, M., 2010. Development of a tundra-specific snow water equivalent retrieval algorithm for satellite passive microwave data. *Remote Sens. Environ.* 114 (8):1699–1709. <http://dx.doi.org/10.1016/j.rse.2010.02.019>.
- Derksen, C., Toose, P., Lemmettyinen, J., Pulliainen, J.T., Langlois, A., Rutter, N., Fuller, M.C., 2012. Evaluation of passive microwave brightness temperature simulations and snow water equivalent retrievals through a winter season. *Remote Sens. Environ.* 117:236–248. <http://dx.doi.org/10.1016/j.rse.2011.09.021>.
- Ding, K.H., Xu, X., Tsang, L., 2010. Electromagnetic scattering by bicontinuous random microstructures with discrete permittivities. *IEEE Trans. Geosci. Remote Sens.* 48 (8): 3139–3151. <http://dx.doi.org/10.1109/TGRS.2010.2043953>.
- Dobson, M.C., Ulaby, F.T., Hallikainen, M.T., El-Rayes, M.A., 1985. Microwave dielectric behavior of wet soil-Part II: dielectric mixing models. *IEEE Trans. Geosci. Remote Sens.* (1):35–46 <http://dx.doi.org/10.1109/TGRS.1985.289498>.
- Du, J., Shi, J., Xiong, C., 2010. A method to estimate Snow Water Equivalent using multi-angle X-band radar observations. Presented at the Geoscience and Remote Sensing Symposium (IGARSS), 2010 IEEE International, Honolulu, HI:pp. 3774–3776 <http://dx.doi.org/10.1109/IGARSS.2010.5651642>.
- Durand, M., Liu, D., 2012. The need for prior information in characterizing snow water equivalent from microwave brightness temperatures. *Remote Sens. Environ.* 126 (C):248–257. <http://dx.doi.org/10.1016/j.rse.2011.10.015>.
- Durand, M., Kim, E.J., Margulis, S.A., 2008. Quantifying uncertainty in modeling snow microwave radiance for a mountain snowpack at the point-scale, including stratigraphic effects. *IEEE Trans. Geosci. Remote Sens.* 46 (6):1753–1767. <http://dx.doi.org/10.1109/TGRS.2008.916221>.
- Durand, M., Kim, E.J., Margulis, S.A., Molotch, N.P., 2011. A first-order characterization of errors from neglecting stratigraphy in forward and inverse passive microwave modeling of snow. *IEEE Geosci. Remote Sens. Lett.* 8 (4):730–734. <http://dx.doi.org/10.1109/LGRS.2011.2105243>.
- Elder, K., Cline, D., Parsons, M., Brodzik, M., 2003. CLPX-Ground: ISA Snow Depth Transects and Related Measurements, Version 2. [Fraser Snowpit Measurements]. NASA National Snow and Ice Data Center Distributed Active Archive Center, Boulder, Colorado USA <http://dx.doi.org/10.5060/D4MW2F23> (Accessed in June 2015).
- Foster, J.L., Hall, D.K., Kelly, R., Chiu, L., 2009. Seasonal snow extent and snow mass in South America using SMMR and SSM/I passive microwave data (1979–2006). *Remote Sens. Environ.* 113 (2):291–305. <http://dx.doi.org/10.1016/j.rse.2008.09.010>.
- Frei, A., Tedesco, M., Lee, S., Foster, J., Hall, D.K., Kelly, R., Robinson, D.A., 2012. A review of global satellite-derived snow products. *Adv. Space Res.* 50 (8):1007–1029. <http://dx.doi.org/10.1016/j.asr.2011.12.021>.
- Gan, T.Y., Kalinga, O., Singh, P., 2009. Comparison of snow water equivalent retrieved from SSM/I passive microwave data using artificial neural network, projection pursuit and nonlinear regressions. *Remote Sens. Environ.* 113 (5):919–927. <http://dx.doi.org/10.1016/j.rse.2009.01.004>.
- Gelman, A., Carlin, J.B., Stern, H.S., Rubin, D.B., 1995. *Metropolis and metropolis-hastings algorithms. Bayesian Data Analysis*, second ed. Chapman & Hall/CRC, Boca Raton, FL, pp. 320–334 (Chapter 11.2).
- Graf, T., Koike, T., Fujii, H., Brodzik, M., Armstrong, R.L., 2003. CLPX-Ground: Ground Based Passive Microwave Radiometer (CBMR-7) Data. NASA DAAC at the National Snow and Ice Data Center, Boulder, Colorado USA (Accessed in June 2015).
- Grody, N.C., Basist, A.N., 1996. Global identification of snowcover using SSM/I measurements. *Geosci. Remote Sens.* <http://dx.doi.org/10.1109/36.481908>.
- Grubbs, F., 2007. Procedures for detecting outlying observations in samples. *Technometrics* 11 (1):1–21. <http://dx.doi.org/10.1080/00401706.1969.10490657>.
- Hallikainen, M.T., Ulaby, F.T., Dobson, M.C., El-Rayes, M.A., Wu, L.-K., 1985. Microwave dielectric behavior of wet soil-part I: empirical models and experimental observations. *IEEE Trans. Geosci. Remote Sens.* 1:25–34. <http://dx.doi.org/10.1109/TGRS.1985.289497>.
- Hallikainen, M.T., Ulaby, F.T., Van Deventer, T.E., 1987. Extinction behavior of dry snow in the 18–90-GHz range. *IEEE Trans. Geosci. Remote Sens.* GE-25 (6):737–745. <http://dx.doi.org/10.1109/TGRS.1987.289743>.

- IGOS, 2007. Integrated Global Observing Strategy Cryosphere Theme Report-for the Monitoring of Our Environment from Space and from Earth. World Meteorological Organization. WMO/TD-No, Geneva, p. 1405.
- Jiang, L., Shi, J., Tjutja, S., Dozier, J., Chen, K., Zhang, L., 2007. A parameterized multiple-scattering model for microwave emission from dry snow. *Remote Sens. Environ.* 111 (2–3):357–366. <http://dx.doi.org/10.1016/j.rse.2007.02.034>.
- Jiang, L., Wang, P., Zhang, L., Yang, H., Yang, J., 2014. Improvement of snow depth retrieval for FY3B-MWRI in China. *Sci. China Earth Sci.* 57 (6), 1278–1292.
- Jordan, R., 1991. A one-dimensional temperature model for a snow cover technical documentation for SNTHERM.89. Cold Regions Research & Engineering Laboratory. Spec. Rep. 91–16, 43–44.
- Kelly, R.E., Chang, A.T., Tsang, L., Foster, J.L., 2003. A prototype AMSR-E global snow area and snow depth algorithm. *IEEE Trans. Geosci. Remote Sens.* 41 (2):230–242. <http://dx.doi.org/10.1109/TGRS.2003.809118>.
- Lemmettyinen, J., Pulliainen, J.T., Rees, A., Kontu, A., Qiu, Y., Derksen, C., 2010. Multiple-layer adaptation of HUT snow emission model: comparison with experimental data. *IEEE Trans. Geosci. Remote Sens.* 48 (7):2781–2794. <http://dx.doi.org/10.1109/TGRS.2010.2041357>.
- Lemmettyinen, J., Kontu, A., Pulliainen, J., Vehviläinen, J., Rautiainen, K., Wiesmann, A., Mätzler, C., Werner, C., Rott, H., Nagler, T., Schneebeli, M., Proksch, M., Schüttemeyer, D., Kern, M., Davidson, M.W.J., 2016. Nordic snow radar experiment. *Geosci. Instrum. Methods Data Syst. Discussions* 5:403–415. <http://dx.doi.org/10.5194/gi-5-403-2016>.
- Liang, D., Xu, X., Tsang, L., Andreadis, K.M., Josberger, E.G., 2008. The effects of layers in dry snow on its passive microwave emissions using dense media radiative transfer theory based on the quasicrystalline approximation (QCA/DMRT). *IEEE Trans. Geosci. Remote Sens.* 46 (11):3663–3671. <http://dx.doi.org/10.1109/TGRS.2008.922143>.
- Matzler, C., 2002. Relation between grain-size and correlation length of snow. *J. Glaciol.* 48 (162):461–466. <http://dx.doi.org/10.3189/172756502781831287>.
- Matzler, C., Wiesmann, A., 1999. Extension of the microwave emission model of layered snowpacks to coarse-grained snow. *Remote Sens. Environ.* 70 (3):317–325. [http://dx.doi.org/10.1016/S0034-4257\(99\)00047-4](http://dx.doi.org/10.1016/S0034-4257(99)00047-4).
- Matzler, C., Schanda, E., Good, W., 1982. Towards the definition of optimum sensor specifications for microwave remote sensing of snow. *IEEE Trans. Geosci. Remote Sens.* GE-20:57–66. <http://dx.doi.org/10.1109/TGRS.1982.4307521>.
- Mironov, V.L., De Roo, R.D., Savin, I.V., 2010. Temperature-dependable microwave dielectric model for an Arctic soil. *IEEE Trans. Geosci. Remote Sens.* 48 (6):2544–2556. <http://dx.doi.org/10.1109/TGRS.2010.2040034>.
- Mocko, D., NASA/GSFC/HSL, 2014. NLDAS VIC Land Surface Model L4 Monthly Climatology 0.125 × 0.125 Degree, Version 002. Goddard Earth Sciences Data and Information Services Center (GES DISC), Greenbelt, Maryland, USA Accessed June 2015. [10.5067/BOL38R609BOR](https://doi.org/10.5067/BOL38R609BOR).
- Montpetit, B., Royer, A., Roy, A., Langlois, A., Derksen, C., 2013. Snow microwave emission modeling of ice lenses within a snowpack using the microwave emission model for layered snowpacks. *IEEE Trans. Geosci. Remote Sens.* 51 (9):4705–4717. <http://dx.doi.org/10.1109/TGRS.2013.2250509>.
- Nijssen, B., Schirnur, R., Lettenmaier, D.P., 2001. Global retrospective estimation of soil moisture using the variable infiltration capacity land surface model, 1980–93. *J. Clim.* 14: 1790–1808. [http://dx.doi.org/10.1175/1520-0442\(2001\)014<1790:GREOSM>2.0.CO;2](http://dx.doi.org/10.1175/1520-0442(2001)014<1790:GREOSM>2.0.CO;2).
- Pan, J., Jiang, L., Zhang, L., 2012. Comparison of the multi-layer HUT snow emission model with observations of wet snowpacks. *Hydro. Process.* 28 (3):1071–1083. <http://dx.doi.org/10.1002/hyp.9617>.
- Pan, J., Durand, M., Sandells, M., Lemmettyinen, J., Kim, E.J., 2016. Differences between the HUT snow emission model and MEMLS and their effects on brightness temperature simulation. *IEEE Trans. Geosci. Remote Sens.* 54 (4):2001–2019. <http://dx.doi.org/10.1109/TGRS.2015.2493505>.
- Picard, G., Brucker, L., Roy, A., Dupont, F., Fily, M., Royer, A., 2012. Simulation of the microwave emission of multi-layered snowpacks using the dense media radiative transfer theory: the DMRT-ML model. *Geosci. Model Dev. Discuss.* 5 (4):3647–3694. <http://dx.doi.org/10.5194/gmdd-5-3647-2012>.
- Picard, G., Brucker, L., Roy, A., Dupont, F., Fily, M., Royer, A., Harlow, C., 2013. Simulation of the microwave emission of multi-layered snowpacks using the dense media radiative transfer theory: the DMRT-ML model. *Geosci. Model Dev.* 6 (4):1061–1078. <http://dx.doi.org/10.5194/gmdd-6-1061-2013>.
- Pulliainen, J.T., 2006. Mapping of snow water equivalent and snow depth in boreal and sub-arctic zones by assimilating space-borne microwave radiometer data and ground-based observations. *Remote Sens. Environ.* 101 (2):257–269. <http://dx.doi.org/10.1016/j.rse.2006.01.002>.
- Pulliainen, J.T., Hallikainen, M.T., 2001. Retrieval of regional snow water equivalent from space-borne passive microwave observations. *Remote Sens. Environ.* 75 (1):76–85. [http://dx.doi.org/10.1016/S0034-4257\(00\)00157-7](http://dx.doi.org/10.1016/S0034-4257(00)00157-7).
- Pulliainen, J.T., Grandell, J., Hallikainen, M.T., 1999. HUT snow emission model and its applicability to snow water equivalent retrieval. *IEEE Trans. Geosci. Remote Sens.* 37 (3):1378–1390. <http://dx.doi.org/10.1109/36.763302>.
- Roberts, G.O., Rosenthal, J.S., 2009. Examples of adaptive MCMC. *J. Comput. Graph. Stat.* 18 (2):349–367. <http://www.jstor.org/stable/25651249>.
- Roy, V., Goita, K., Royer, A., Walker, A.E., Goodison, B.E., 2004. Snow water equivalent retrieval in a Canadian boreal environment from microwave measurements using the HUT snow emission model. *IEEE Trans. Geosci. Remote Sens.* 42 (9):1850–1859. <http://dx.doi.org/10.1109/TGRS.2004.832245>.
- Sturm, M., Holmgren, J., Liston, G.E., 1995. A seasonal snow cover classification system for local to global applications. *J. Clim.* 8 (5):1261–1283. [http://dx.doi.org/10.1175/1520-0442\(1995\)008<1261:ASSCCS>2.0.CO;2](http://dx.doi.org/10.1175/1520-0442(1995)008<1261:ASSCCS>2.0.CO;2).
- Sturm, M., Taras, B., Liston, G.E., Derksen, C., Jonas, T., Lea, J., 2010. Estimating snow water equivalent using snow depth data and climate classes. *J. Hydrometeorol.* 11 (6): 1380–1394. <http://dx.doi.org/10.1175/2010JHM1202.1>.
- Takala, M., Luojus, K., Pulliainen, J.T., Derksen, C., Lemmettyinen, J., Kärnä, J.-P., et al., 2011. Estimating northern hemisphere snow water equivalent for climate research through assimilation of space-borne radiometer data and ground-based measurements. *Remote Sens. Environ.* 115 (12):3517–3529. <http://dx.doi.org/10.1016/j.rse.2011.08.014>.
- Tedesco, M., Kim, E.J., 2006. Retrieval of dry-snow parameters from microwave radiometric data using a dense-medium model and genetic algorithms. *IEEE Trans. Geosci. Remote Sens.* 44 (8):2143–2151. <http://dx.doi.org/10.1109/TGRS.2006.872087>.
- Tedesco, M., Pulliainen, J.T., Takala, M., Hallikainen, M.T., Pampalon, P., 2004. Artificial neural network-based techniques for the retrieval of SWE and snow depth from SSM/I data. *Remote Sens. Environ.* 90 (1):76–85. <http://dx.doi.org/10.1016/j.rse.2003.12.002>.
- Tsang, L., Kong, J.A., 2001. *Multiple scattering theory for discrete scatterers. Scattering of Electromagnetic Waves - Advanced Topics*. John Wiley & Sons, Inc, New York, pp. 197–241 (Chapter 5).
- Tsang, L., Pan, J., Liang, D., Li, Z., Cline, D.W., Tan, Y., 2007. Modeling active microwave remote sensing of snow using dense media radiative transfer (DMRT) theory with multiple-scattering effects. *IEEE Trans. Geosci. Remote Sens.* 45 (4):990–1004. <http://dx.doi.org/10.1109/TGRS.2006.888854>.
- Ulaby, F.T., Long, D.G., 2014. *Emission by snow-covered terrain. Emission Models and Land Observations, Microwave Radar and Radiometric Remote Sensing*. The University of Michigan Press, Ann Arbor, MI, USA, pp. 586–595 (Chapter 12–11).
- Van Kempen, G.M., Van Vliet, L.J., 2000. Mean and variance of ratio estimators used in fluorescence ratio imaging. *Cytometry* 39 (4):300–305. [http://dx.doi.org/10.1002/\(SICI\)1097-0320\(20000401\)39:4<300::CO;2-0](http://dx.doi.org/10.1002/(SICI)1097-0320(20000401)39:4<300::CO;2-0).
- Wegmüller, U., Matzler, C., 1999. Rough bare soil reflectivity model. *IEEE Trans. Geosci. Remote Sens.* 37 (3):1391–1395. <http://dx.doi.org/10.1109/36.763303>.
- Wiesmann, A., Matzler, C., 1999. Microwave emission model of layered snowpacks. *Remote Sens. Environ.* 70 (3):307–316. [http://dx.doi.org/10.1016/S0034-4257\(99\)00046-2](http://dx.doi.org/10.1016/S0034-4257(99)00046-2).
- Wiesmann, A., Matzler, C., Weise, T., 1998. Radiometric and structural measurements of snow samples. *Radio Sci.* 33 (2):273–289. <http://dx.doi.org/10.1029/97RS02746>.
- Xu, X., Tsang, L., Yueh, S., 2012. Electromagnetic models of co/cross polarization of bicontinuous/DMRT in radar remote sensing of terrestrial snow at X- and Ku-band for CoReH<sub>2</sub>O and SCLP applications. *IEEE J. Sel. Top. Appl. Earth Observ. Remote. Sens.* 5 (3):1024–1032. <http://dx.doi.org/10.1109/JSTARS.2012.2190719>.
- Yardim, C., Gerstoft, P., Hodgkiss, W.S., 2006. Estimation of radio refractivity from radar clutter using Bayesian Monte Carlo analysis. *IEEE Trans. Antennas Propag.* 54 (4): 1318–1327. <http://dx.doi.org/10.1109/TAP.2006.872673>.